Institute for Computer Science VII
Robotics and Telematics

Master's thesis

Development of an automated adjusting process for robotic end-effectors to handle dry textiles for preforming of carbon fiber reinforced plastics

Robin Leblebici

January 2018

First examiner:	Prof. Dr. Andreas Nüchter (JMUW)
Second examiner:	Prof. George Nikolakopoulos (LTU)
Supervisor:	M. Sc. Dominik Deden (DLR)

Abstract

In order to fulfill increasing production rates, new automated production technologies are required for manufacturing carbon fiber reinforced plastic components for the aerospace industry. Currently, large, double curved composite components have to be manufactured manually, which leads to high process times and poor scalability. As a consequence, a team of cooperating robots with passively adjustable end-effectors was developed, that is capable of handling dry carbon textiles and can be used for layups in double curved molds. This thesis deals with the implementation of a robot program, that performs an automated adjustment of each end-effector to the surface geometry of the manufactured part. The functional principle and the accuracy of the process are evaluated. Further, the automatically adjusted end-effectors are utilized to cooperatively layup carbon plies. The results show, that the accuracy of the automated adjusting process is sufficient to drape carbon fabrics during pick-up and automated layup is possible with this approach. In conclusion, the developed process can be integrated into a fully automated process for future experiments, but hardware inaccuracies should be improved, in order to further enhance the accuracy of the system.

Contents

Chapter 1

Introduction

The demand for aircrafts operated in civil air traffic has increased over recent years. As of late 2017, Airbus received a total of 6141 open orders for aircrafts of the A320 family [1] with a current production rate of less than 60 aircrafts per month [2]. Thus, a production ramp-up is required in order to full-fill the steep demand, which promotes research in new automated production technologies. For the future, the lifespan of a modern airplane is expected to be 30+ years, thus especially longevity, fuel efficiency and weight reduction play a major role in the designing stage. In general, decreasing the weight has a great impact on the performance over the lifetime of an aircraft, thus lightweight construction technologies are increasingly used for aircraft manufacturing. Currently, one approach is to make use of carbon fiber reinforced plastic (CFRP) for structural components. As an example, the airframe of an Airbus A350 XWB released in 2015 is made of 53 % of CFRP[19]. However, many CFRP-manufacturing techniques require manual labour, that is complex and time-consuming. At the same time, high accuracy is demanded throughout the process. In order to full-fill the increasing production rates, the Center for Lightweight Production Technologies of the German Aerospace Center (DLR) in Augsburg is invested in developing innovative automated manufacturing techniques in cooperation with the aerospace industry.

The underlying manufacturing technique utilized in this work is a thermoset process. It consists of creating a preform from cut dry carbon-fiber textiles that are later infused with resin in a vacuum-assisted process. During this process, several differently shaped pre-cut layers of carbon-fiber have to be placed and draped in a tool that is used to create the preform. So far, the cut carbon fiber pieces are often handled manually. Especially for large structural components, such as fuselage panels and pressure bulkheads, this leads to problems, for example non-ergonomic handling positions during the manual draping process and high process times. Additionally, reproducibility has to be guaranteed, which could otherwise weaken the structural integrity of manufactured parts. Thus, replacing manual handling of cut carbon fabrics is one of many goals of the automated manufacturing process. For that purpose, robotic end-effectors are being developed that are capable of draping cut pieces of carbon fiber during pick-up and placing them automatically in a formative tool.

A process that relies on a team of cooperating robots was developed to be capable of handling large pieces of carbon fiber fabrics. The advantage of handling large plies lies in higher achievable layup rates and shorter process times. However, a challenge lies in the different shapes and sizes of the cut textile layers, as well as the different tool geometries of the manufactured parts. As a consequence, an end-effector was developed, that can be passively adjusted to the required shape of the tool geometry and is used in this work. The main feature of the robotic end-effector, is its ability to adjust its shape to double curved surface geometries. This is achieved by an end-effector that consists of identically constructed pneumatic elements interconnected by ball joints, which can be passively adjusted by a dedicated adjusting station controlled by the robots. The automatic adjustment is the focus of this work, which is supposed to be integrated into the fully automated manufacturing process of a pressure bulkhead for the Airbus A350.

1.1 Goals and outline

The purpose of this Master's thesis is to develop a process that is capable of adjusting the robotic end-effectors passively in conjunction with an adjusting station. As a result, the shape of the end-effector has to match the predefined double curved surface geometry of a tool. This enables all functionalities (e.g. draping, placing) for the fully automated manufacturing process. Thus, the development of a robot program was realized, that controls the mechanical components of the adjusting station and automatically adjusts each element of the end-effector to its predefined orientation. In order to handle plies of various geometries in a consecutive process, the program needs to be capable of adjusting the end-effector from a previously adjusted state. Additionally, the program has to plan the robot's path according to boundary conditions resulting from the spatial limitation of the robotic end-effector during the interaction with the measuring sensors of the adjusting station.

First, chapter 2 introduces current CFRP manufacturing techniques for composite components and highlights the challenges of an automated process.
The end-effector and the necessary components of the adjusting station are described in section 3.1. Also, a basic overview of the robot programming software is given in section 3.2.
The functional principle of the measuring and adjusting process is described in section 4.1, as well as the determination of the end-effector shape from the 3D model in section 4.2. Additionally, the electrical controlling of the mechanical components is explained in section 4.3.
Further, the accuracy of the developed adjusting process is evaluated and discussed in chapter 5 and a conclusion is given in chapter 6.

Chapter 2

State of the Art

Numerous methods for fabricating composite components exist today. Many of them were developed to meet specific design or manufacturing challenges. The following chapter highlights automated manufacturing techniques for composite materials and compares them to the manual process. However, not every fabrication technique is explored, instead the focus lies on processes for automated manufacturing of large components with double curved geometries. An example are pressure bulkheads and fuselage panels of aircrafts, as shown in figure 2.1. Further, the challenges that lie in handling large fabric layers during the automated preforming process are presented.

2.1 Composite manufacturing techniques

Composite fabrication processes require a formative geometry to give the unformed resin and fiber material its shape and form the outer profile of the composite component. The formative tool is usually called a mold. At the beginning of the process, dry layers of pre-cut fabric (also referred to as plies) are placed into the open mold and draped to create a preform. In CFRPs, carbon fibers serve as the reinforcement of the composite component, which provides its strength and rigidity. After layup is complete, resin is injected into the dry fabrics that serves as a binding matrix to bind the reinforcements together and distribute forces between the carbon fibers [7]. Then, the composite material has to be cured, either by applying heat or pressure by means of a vacuum, resulting in a part referred to as thermoset composite.

A variation to this technique is called wet lay-up. Here, plies which are pre-impregnated with resin (also referred to as pre-pregs [20]) are used. Pre-pregs are partially cured to allow easy handling, but still require debulking after layup is complete. This is commonly achieved by a vacuum-bagging technique that uses sealed plastic sheets on top of the preform around the tool, which consolidates the layup. Since heat accelerates the curing process, pre-pregs are commonly placed in an oven or autoclave to cure. Additionally, pre-pregs require cold storage to prevent them from curing beforehand. As a consequence, handling and storage of pre-pregs is expensive, compared to dry fiber materials. However, this fabrication method is especially useful for small parts with complex geometries, that have to be layed-up of many differently shaped plies.

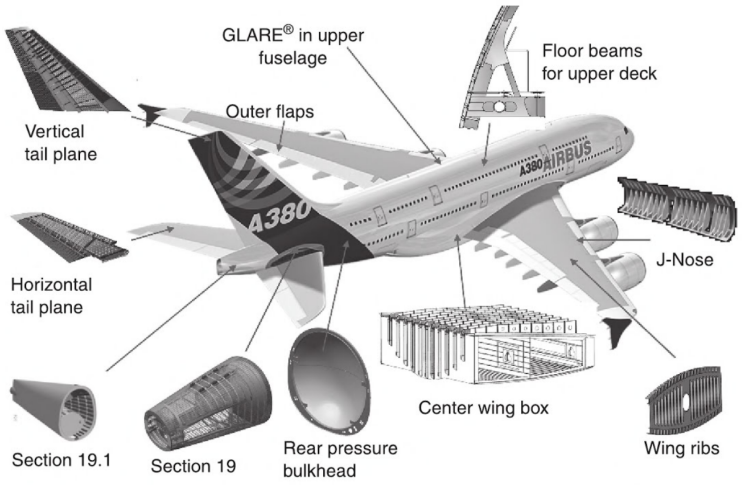

Figure 2.1: Overview of composite components in an Airbus A380 [17].

Draping
Both techniques require the textile layers to be placed into the double curved mold to form a laminate stack. For that purpose, the fibers of the 2D fabric layers have to adapt to the 3D form in a process commonly referred to as draping. In general, carbon fiber fabrics exhibit low shear and bending stiffness, which allows them to adapt to complex, double curved surface geometries [18]. This enables the final composite component to feature a specific fiber structure and orientation, allowing it to transfer forces more efficiently. Thus, draping serves as an essential step during composite manufacturing and greatly influences the quality of composite components. During draping, it is essential to avoid deformation to the fibers inside the fabric, such as wrinkling or bridging. Material tensions should be avoided, in order to maintain the mechanical properties and the specific fiber orientation of the final composite component.

A common method of draping fabric layers is hand layup. During the process, draping is accomplished manually by workers with the help of rollers and brushes, as shown in figure 2.3 (right). However, a challenge lies in handling large plies (e.g. 4 m x 1 m), when using manually intensive lay-up techniques. Large plies are difficult to handle ergonomically, as shown in figure 2.3 (left), which results in high process times. In addition to that, draping of large fabric layers is difficult to reproduce in a manual process, thus yielding a poor reproducibility, since in many cases fiber deformations occur, that weaken the internal structure of the composite component [11]. As a consequence, the ever-increasing demand for faster production rates urges to replace hand layup with automated fabrication processes, as presented in the following section.

2.2 Automated preforming

One approach to minimize process times is to create layups of large dry fabrics automatically in conjunction with robotic end-effectors. The automated material handling is derived from the manual process, where several workers pick-up, transport, position and drape a fabric layer

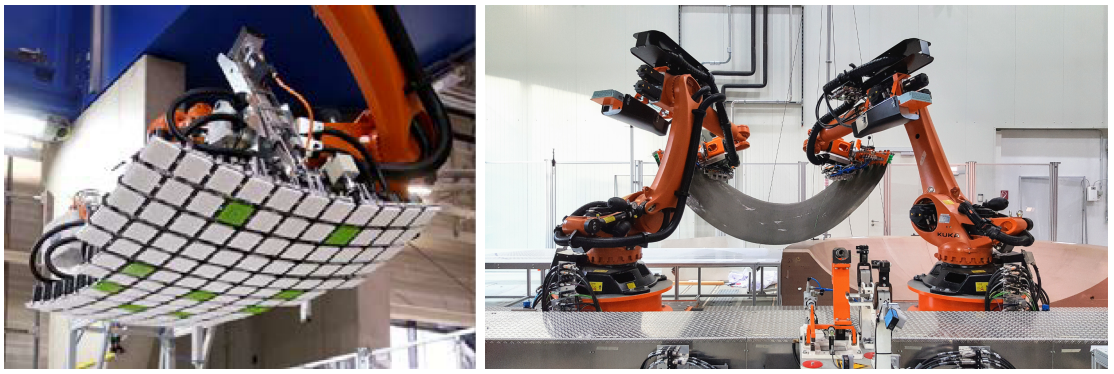

Figure 2.2: Robots using different pick and place techniques of carbon fabric layers. Single actively adjustable end-effector (left) [8], two cooperating passively adjustable end-effectors transporting a draped fabric layer (right) [5].

from a table onto a tooling. For that purpose, robotic end-effectors are being developed, which are built of individual modules, that can be adjusted to the target geometry. With these end-effectors, fabric layers can be handled similar to the manual process.
At the start of an automated process, the pre-cut fabric layers are usually picked up from a flat surface. In order to be able to place fabric layers accurately into a mold, the fabrics have to match the shape of the mold priorly. Thus, the end-effectors have to be capable of draping the fabric layers during or after pick-up, which requires the end-effectors to be adjustable and adapt to the surface geometry of the mold.

One technique that uses an actively adjustable end-effector is shown in figure 2.2 (left). Picking up fabric layers from a flat surface is possible with a straightened end-effector. Thereupon, the single elements of the gripper are actively controlled and can be mapped to resemble a curve with a set radius. Thus, draping of a fabric layer is possible after it is picked up.
This has advantages regarding process time and handling of the carbon plies, but requires a complex controlling system of the end-effector. Thus, the maximum size of fabric layers the end-effector can handle is limited due to its size and complex design. [8]

A different approach is to use two cooperating robots, as shown in figure 2.2 (right). Here, the end-effector is only passively adjustable, which requires it to be adapted to the surface geometry of the mold before it is used pick-up the fabric layer. This requires a complex pick-up technique, that passively drapes the fabric layer to its required shape. This was proven to be possible in a semi-automated process [5], in which the end-effectors were adjusted manually.
One characteristic of this technique is, that larger pieces of fabric layers and double curved geometries can be handled, which has advantages regarding production volume and scalability. However, for a fully automated manufacturing process, an automated adjustment is required that precisely adapts the shape of the end-effector to the surface geometry of the mold, in order to ensure the accuracy needed in an industrialized production.

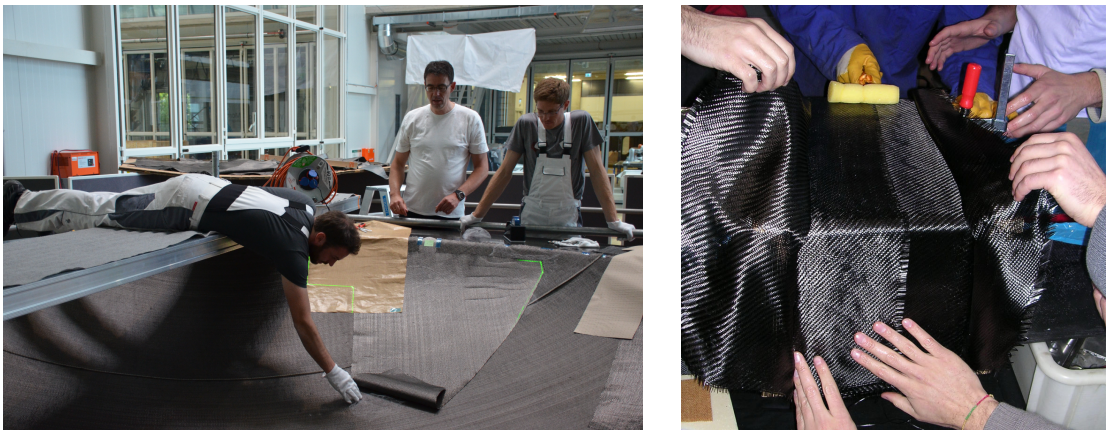

Figure 2.3: Manual hand layup of a carbon fabric layer onto a mold using laser projection (left), required tools during hand layup (right).

Layup positioning and transportation

Furthermore, positioning of the plies is important to the final quality of the composite component. During a manual process, laser projection systems are used to project the outline of large pre-cut fabrics onto the mold, as shown in figure 2.3 (left). Robots are superior in positioning objects in Cartesian space. Therefore, positioning of the plies in the mold according to the data from computer-aided design (CAD) can be achieved more accurately. As a consequence, the reproducibility is higher compared to the manual layup process. However, cooperating robots require synchronization of their movements, in order to maintain the shape of the fabric acquired during the draping process. Because of that, a geometrical link has to be established between the robots, which commands one robot (slave) to follow the movements of the other robot (master). At the current state of the art, this is possible by KUKA's RoboTeam technology [13]. All of this is necessary for two or more robots in order to perform cooperating motions, which would otherwise result in unreliable movements and collisions, that could also damage the fabric layers. In order to transport the fabric layers from one location to another, the robots are commonly mounted on a linear axis to extend their work envelope.

Chapter 3

Technical background

This chapter offers necessary background information about the deployed mechanical components, such as the robot cell and the adjustable robotic end-effector. Further, it introduces common terms and mathematical conventions used in robotics and throughout this thesis.

3.1 Hardware

The following section gives an overview of hardware components necessary for adjusting the robotic end-effector. Thus, it specifies the properties of the robot cell, the adaptive robotic gripper and the adjusting station. Additionally, it describes the functional principle of the adjusting process from a mechanical point of view and highlights its challenges.

3.1.1 Robot cell

The robot cell for technology testing at DLR consists of two KUKA KR 210 R3100 ultra robots (called R1 and R2) with a maximum load of 210 kg mounted on a linear external axis. The cell is depicted in figure 3.1. Also shown is the adjusting station developed by KUKA Systems and DLR, which is integrated into the cell and directly connected to the robots. It is actuated

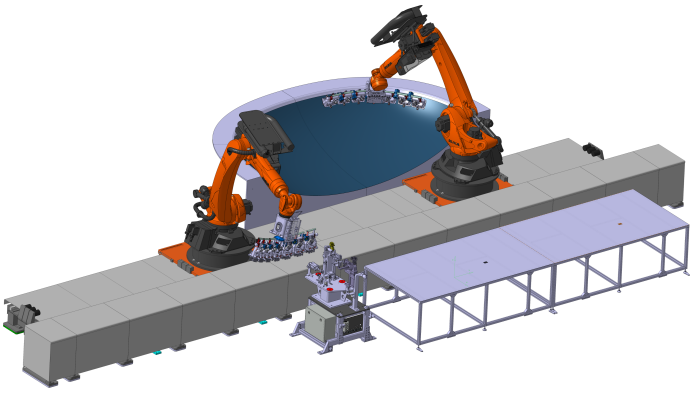

Figure 3.1: The robot cell - adjusting station (front) next to calibrated tables used for pick-up of fabric layers, robots on linear axis (center) and mold (back).

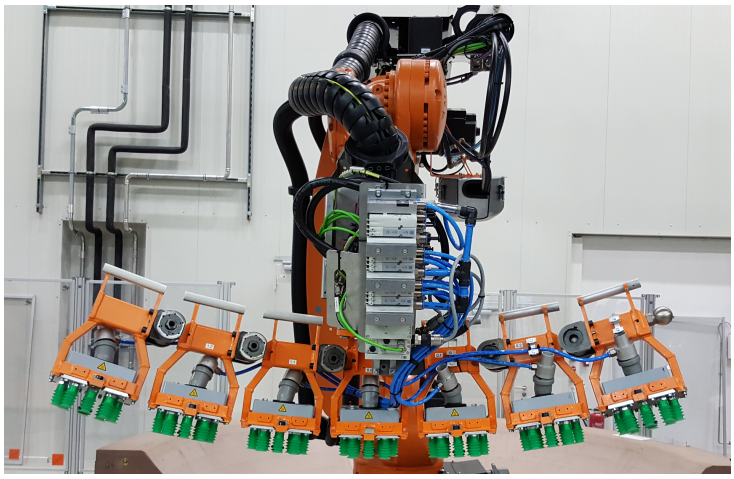

Figure 3.2: The adjustable robotic end-effector.

by the KUKA robot control (KRC) of the robots and enables the adjustment of both robotic end-effectors. From two measured and calibrated tables, the pre-positioned fabric layers of dry carbon fiber can be picked up cooperatively by the two robots. For the purpose of placing down the fabric layers onto a mold, a test geometry with double curved surfaces is used, which resembles the geometry of a pressure bulkhead.

3.1.2 Adjustable robotic end-effector

The main purpose of the robotic end-effector lies in its ability to pick up large plies of carbon-fiber fabrics while simultaneously draping the plies with a specific pick-up motion. The end-effector itself, as depicted in figure 3.2, consists of several identically constructed elements interconnected by ball joints. These joints can be tightened and loosened and allow each element to be adjusted in three rotary degrees of freedom. These are further referred to as the set-angles of each joint. This allows the robotic gripper to adapt its shape to double curved surface geometries, which is required to drape a fabric layer and place it into a mold. However, the central element of the end-effector is fixed via a link to the robot flange, thus its position is always known relative to the robot flange and is used as a reference.

Figure 3.3 shows a singular isolated element and highlights its basic components. Fixed to the topside of each element is a measurement tube. It is used in conjunction with the sensors of the measuring station to determine the orientation of each element. A detailed description of the measurement process can be found in section 4.1.2.
Gripping and picking up fabric layers is done by the principle of volume flow. For that purpose, 11 suction cups are located at the bottom side of each element. They are controlled pneumatically by a central valve terminal connected to the center element of the end-effector, as shown in figure 3.2. In previous works [15][21] it was shown, that suction cups are appropriate to handle air-permeable carbon fiber fabrics.
Attached to the side of each element is a fixing collar bushing that is used to clamp down the

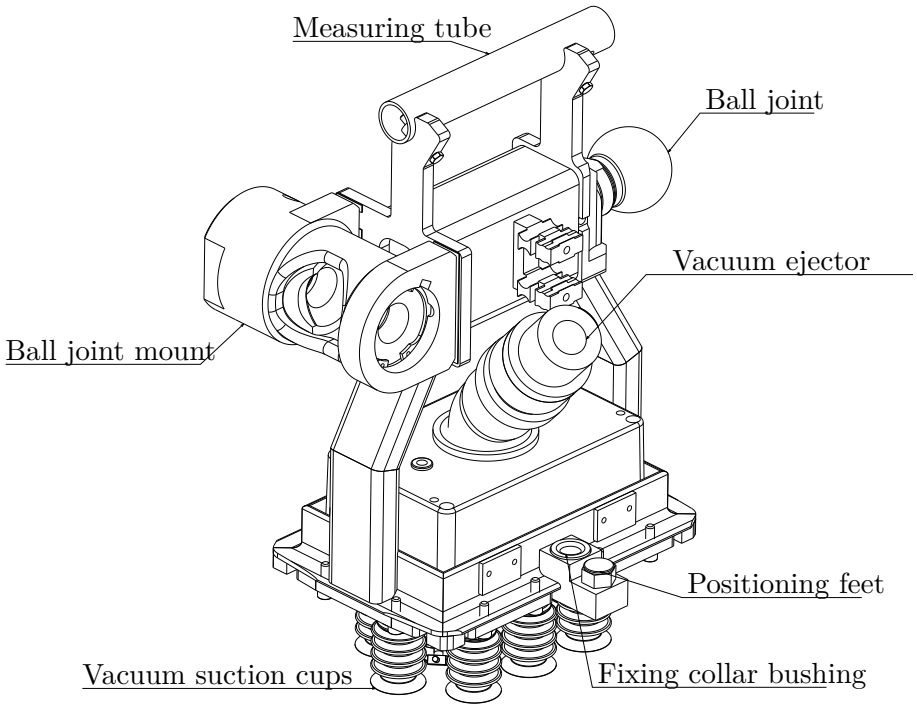

Figure 3.3: Isometric overview of an isolated gripper element showing the basic components.

element during the adjusting process, so that its position stays fixed while its joint is loosened. Also a positioning foot is affixed next to the collar bushing on each side to hold the element into place more precisely. A detailed description of the adjusting process can be found in the next chapter in section 4.1.3.

The ball joint of each element is simply attached to the ball joint mount of its preceding element, which provides a mechanical fixture that holds the element in place when tightened. The end-effector was designed with a maximum of four elements per side. However, increasing the number of elements results in a larger interfering contour and also decreases the accuracy of the adjusting process, as evaluated in chapter 5. For the current geometry of a pressure bulkhead only three elements per side are required, thus the number of elements was reduced.
Due to the interfering contour and mechanical constraints of the robotic end-effector and the adjusting station, the work envelope of the robot yields an upper limit for the maximum set-angles each element can be adjusted to.

3.1.3 Adjusting station

The adjusting station serves as an interface to connect all mechanical, electrical and pneumatic components necessary for the adjustment process to the robot. An overview of the components is shown in figure 3.4. The adjusting station consists of two retro-reflective sensors (Sick WT27L-2F430 [23]) with a measurement frequency of 1000 Hz, which are used to measure the orientation of each element. A detailed explanation of the measurement principle is given in section 4.1.2.

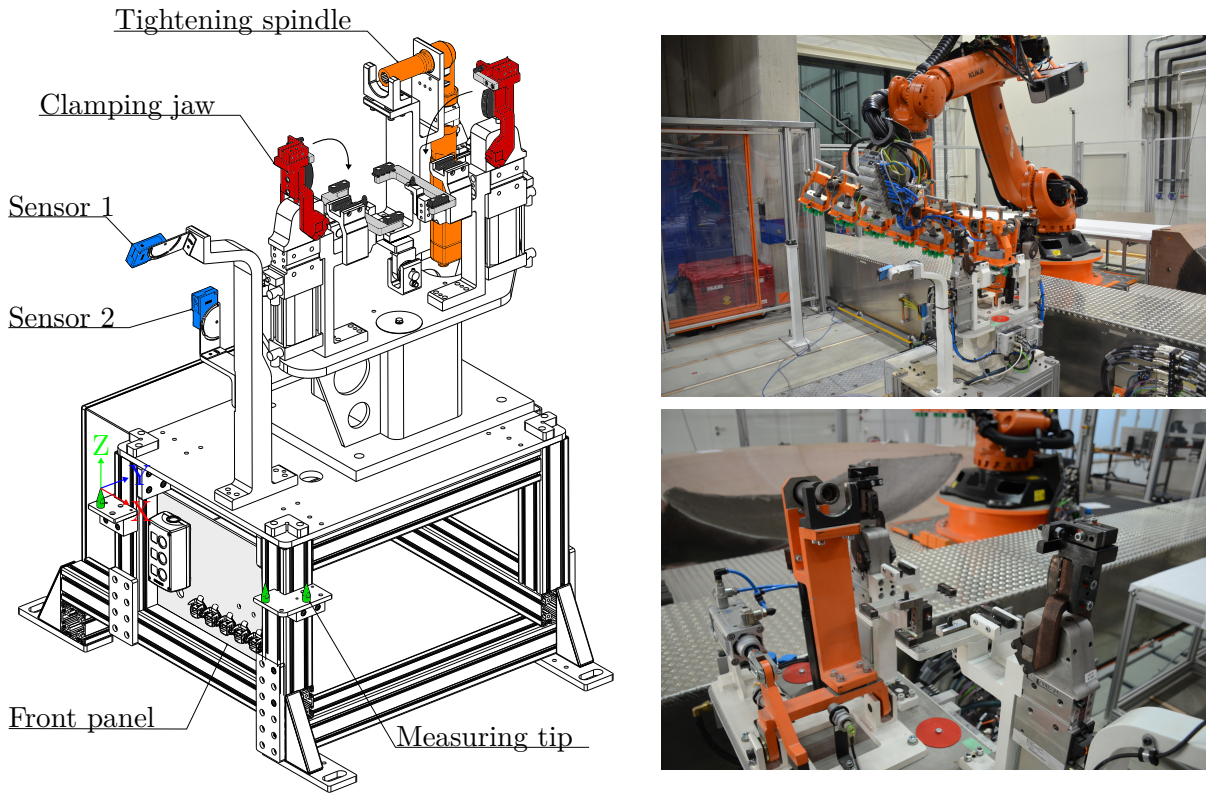

Figure 3.4: CAD drawing of adjusting station with highlighted essential components (left), robotic end-effector position during adjusting process (top right), close-up of clamping position and support surface (bottom right).

Two pneumatically controlled lock-down clamping jaws are used to fix an element in place. An attachable tightening spindle is deployed to loosen and tighten the ball joint connection between two elements. The adjustment of each element is done passively with the help of the robot's motion. A detailed explanation of the adjustment process is described in section 4.1.3.

From a mechanical point of view, the adjusting process for a single element works as follows: First, the sensors have to be used to measure the angular deviation between the element and the orientation of the support surface of the clamping position. The element is then aligned with, and lowered onto the support surface, where two guiding pins slide into the collar bushings of the element from below to secure its position. Afterwards, the tightening spindle can be attached to the screw head of the ball joint and used to loosen the joint. Locking-down the clamping jaws will then press-fit two additional pins into the collar bushings from above, which interlock and fix the element into place. In this state, the robot can be moved to adjust the orientation of the ball joint. However, the motion of the robot is highly restricted in this state, since no translatory movements are permitted, which would otherwise result in damaged components. Thus, a solely circular motion about the ball joint of the fixed element is required, which limits the degrees of freedom of the robot from six to three. The rotary motion is further described in section 4.1.3.

After the adjustment, the tightening spindle tightens the ball joint again, which fixes the connection between the two elements. The clamping jaws are then released, so that the robot can lift up the element out of the clamping position and repeat the adjusting process for the next element. The order of adjustments important, since consecutive elements are mutually dependent on each other. Thus, the adjustments have to be made from the inner to the outer elements.
Originally, the adjusting station and the measurement station were two separate units designed by KUKA systems. In a previous work [9], they were re-designed and all components were merged into a single unit. This allowed the station to be moved conveniently to a different robot cell, but required the robot program to be rewritten since the geometry and the interface connections changed, which are now located at a single front panel of the adjusting station.

3.1.4 Modifications

Two modifications were made compared to the previous hardware state of the adjusting station. First, the guiding pins of the clamping position are now movable. This helps finding the right clamping position, which has to satisfy the clamping jaws and the tightening spindle.
Secondly, the sensors are now more rigidly connected to the station which prevents unwanted movement that would result in inaccuracies during the measurement process, which was not the case previously. Also, the top sensor is now mounted on an shaft, which is adjustable, so that the two sensors properly intersect in an intersection point. This is necessary to ensure proper functioning of the measuring process.

3.2 Robot programming

The underlying programming language used to control KUKA robots is the so called KUKA Robot Language (KRL). It utilizes some specific conventions, coordinate systems and variables which resemble common terms in the field of robotics. For the sake of completeness, and since these will be used throughout this thesis, they are summarized in this section.

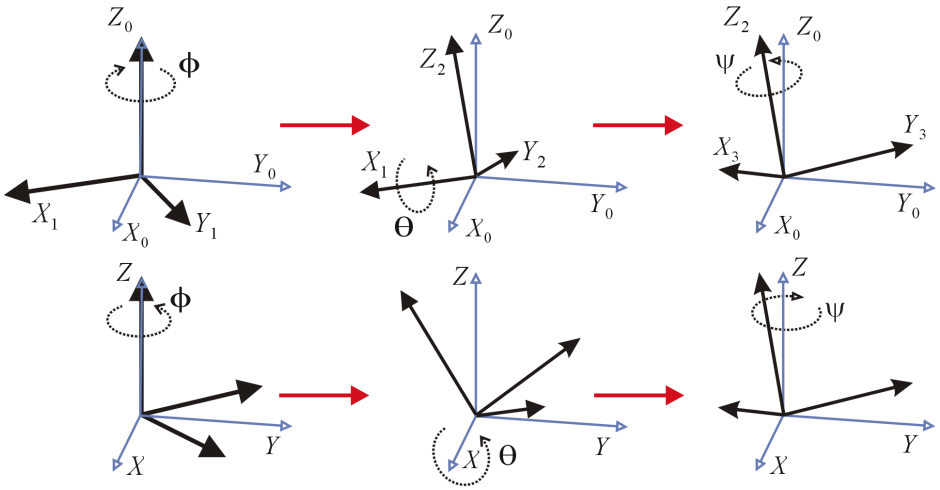

Figure 3.5: Intrinsic rotation (top) compared to extrinsic rotation (bottom).

3.2.1 Position and orientation representation

To define position and orientation in 3D space, KRL utilizes so called coordinate frame variables. A frame is a minimal representation of all six degrees of freedom (DoF) of a rigid body in 3D space. It consists of a position vector $\overrightarrow{p} = [x, y, z]$ and three Euler angles $\angle$(A, B, C) to determine orientation. Usually, ψ, θ and ϕ are chosen to describe the Euler angle rotation about the X-, Y- and Z-axis. However, KRL uses A, B, and C, where A describes the rotation about the Z-axis, B about the Y-axis and C about the X-axis. Thus, the elemental rotation matrices are defined as follows:

$$
\begin{aligned}
R_Z(A) &= \begin{pmatrix} \cos(A) & -\sin(A) & 0 \\ \sin(A) & \cos(A) & 0 \\ 0 & 0 & 1 \end{pmatrix} \\
R_Y(B) &= \begin{pmatrix} \cos(B) & 0 & \sin(B) \\ 0 & 1 & 0 \\ -\sin(B) & 0 & \cos(B) \end{pmatrix} \\
R_X(C) &= \begin{pmatrix} 1 & 0 & 0 \\ 0 & \cos(C) & -\sin(C) \\ 0 & \sin(C) & \cos(C) \end{pmatrix}
\end{aligned}
\tag{3.1}
$$

In general, a convention is required which defines the order of successive elemental rotations when working with Euler angles. Out of the 12 possible orders of rotation, KRL uses the Z-Y-X Euler convention with intrinsic rotations.
To give a better understating of Euler rotations, first we have to define two coinciding coordinate frames. One is a fixed reference frame, that is not moved, and the other one is representing the rotating coordinate system, also called mobile frame. Consecutively rotating the mobile frame about the fixed axes of the reference coordinate frame is defined as extrinsic rotation. On the contrary, rotating the mobile frame about its own axis after each rotation is called intrinsic rotation. The difference is depicted in figure 3.5.
By definition, extrinsic rotation require pre-multiplication of elemental rotation matrices, whereas intrinsic rotations require post-multiplication. This yields the following order of matrix multiplications for the above mentioned Z-Y-X Euler convention with intrinsic rotations in KRL:

$$
R = R_Z(A) \cdot R_Y(B) \cdot R_X(C), \tag{3.2}
$$

which results in the following rotation matrix R:

$$
\begin{pmatrix} \cos(A)\cos(B) & \cos(A)\sin(B)\sin(C) - \sin(A)\cos(C) & \cos(A)\sin(B)\cos(C) + \sin(A)\sin(C) \\ \sin(A)\cos(B) & \sin(A)\sin(B)\sin(C) + \cos(A)\cos(C) & \sin(A)\sin(B)\cos(C) - \cos(A)\sin(C) \\ -\sin(B) & \cos(B)\sin(C) & \cos(B)\cos(C) \end{pmatrix} \tag{3.3}
$$

The Euler angles can be retrieved from the rotation matrix by the following equations:

$$\begin{aligned} B &= \operatorname{atan2}\left(-R_{31}, \sqrt{R_{11}^2 + R_{21}^2}\right) \\ A &= \operatorname{atan2}\left(\frac{R_{32}}{\cos(B)}, \frac{R_{33}}{\cos(B)}\right) \\ C &= \operatorname{atan2}\left(\frac{R_{21}}{\cos(B)}, \frac{R_{11}}{\cos(B)}\right) \end{aligned} \tag{3.4}$$

Also, it should be noted that by reversing the order of rotation and simultaneously switching the method of rotation (intrinsic $\leftrightarrow$ extrinsic), we get the same final orientation (given the same Euler angles). Thus Z-Y-X with intrinsic rotations results in the same orientation as X-Y-Z with extrinsic rotations. [22, p. 12]

3.2.2 Homogeneous transformations

Combining position and orientation in a compact notation, is commonly achieved by using homogeneous transformation matrices. A homogeneous transformation matrix is a 4×4 matrix defined as follows:

$$^{j}T_i = \begin{pmatrix} R & p \\ \eta^T & \sigma \end{pmatrix} \tag{3.5}$$

Where R, p, η^T and σ are defined as:

$$\begin{aligned} R \in \mathbb{R}^{3\times3} &: \text{Rotation matrix.} \\ p \in \mathbb{R}^{3\times1} &: \text{Translation vector.} \\ \sigma \in \mathbb{R} &: \text{Scaling factor (usually equals 1).} \\ \eta^T \in \mathbb{R}^{1\times3} &: \text{Perspective vector (usually zero vector } \overrightarrow{0}\text{).} \end{aligned}$$

In this notation, the homogeneous transformation matrix $^{j}T_i$ transforms a vector from coordinate frame i to coordinate frame j, and also yields the orientation of frame i relative to frame j. Thus, it can effectively be used to transform a coordinate frame into a different coordinate system.
A common notation to describe e.g. a rotation about the Y-axis by angle B is often denoted as follows:

$$T_{rot}(Y, B) = \begin{pmatrix} \cos(B) & 0 & \sin(B) & 0 \\ 0 & 1 & 0 & 0 \\ -\sin(B) & 0 & \cos(B) & 0 \\ 0 & 0 & 0 & 1 \end{pmatrix} \tag{3.6}$$

The homogeneous transformation of a translation along the Z-axis about d can similarly be denoted by the following expression:

$$T_{trans}(Z,d) = \begin{pmatrix} 1 & 0 & 0 & 0 \\ 0 & 1 & 0 & 0 \\ 0 & 0 & 1 & d \\ 0 & 0 & 0 & 1 \end{pmatrix} \tag{3.7}$$

Compositions of homogeneous transformation matrices allow arbitrary coordinate frames to be rotated and translated at the same time. This is achieved by simple matrix multiplication of two homogeneous matrices. Since matrix multiplications are not commutative, the order of multiplication sequence is important, just as in case of rotation matrices. This enables to calculate complex geometrical operations, such as translating and rotating a frame about up to three axes simultaneously.

If a frame F_0 is transformed multiple times ($i = 1, \ldots, n$), every transformation is applied to the previously transformed coordinate system. Thus, each transformation has to be defined with respect to the current frame F_{i-1}. Then the final position of frame F_n relative to frame F_0 can be deduced by post-multiplying all transformation matrices consecutively:

$$^0T_n = {}^0T_1 \cdot {}^1T_2 \cdot \ldots \cdot {}^{n-1}T_n \tag{3.8}$$

On the other hand, transformations between coordinate frames require pre-multiplication. For example a transformation from frame i to frame k via a common basis j can be expressed as follows:

$$^kT_i = {}^kT_j \cdot {}^jT_i \tag{3.9}$$

Also, the inverse of a homogeneous transformation matrix $^jT_i^{-1}$ can be calculated, which transforms vectors from coordinate frame j to coordinate frame i, by the following equation:

$$^jT_i^{-1} = {}^iT_j = \begin{pmatrix} R^T & -R^T p \\ \eta^T & \sigma \end{pmatrix} \tag{3.10}$$

Thus, the inverse of a homogeneous transformation matrix can be used to reverse a transformation. Regarding rotations it can be thought of as rotating in the opposite direction of the original transformation. [6]

Geometric-operator
Technically, a homogeneous transformation matrix consists of 16 elements, but can be derived solely from the minimal six DoF representation: Position vector $\overrightarrow{p} = [x, y, z]$ and Euler angles $\angle$(A, B, C), given a specific Euler convention.
Thus, for simplification, KRL offers a defined geometric-operator, with the following notation:

$$T_{\text{frame}}(F_1, F_2) = (T_1 : T_2) \tag{3.11}$$

It takes two frame variables $F_1, F_2 \in$ (X,Y,Z,A,B,C) as an input, which consists of position vector $\overrightarrow{p}$ and orientation vector in Euler convention. Then, it constructs the homogeneous multiplication matrix T_1 and T_2 from both frames, performs the multiplication and outputs the result as a new frame. If a frame consists of a position and orientation vector, which are both not trivial ($\overrightarrow{0}$), the coordinate frame is always first translated and then rotated in the original frame of reference. This is due to the way homogeneous transformation matrices are constructed in KRL, which implements the following order for homogeneous matrix multiplication:

$$T = T_{trans}(\overrightarrow{p}, \overrightarrow{p}) \cdot T_{rot}(z, A) \cdot T_{rot}(y, B) \cdot T_{rot}(x, C) \tag{3.12}$$

As an example, the inverse of a homogeneous transformation matrix can be used to calculate the difference in orientation between two coordinate frames. Here, ${}^1T_2$ describes the necessary transformation, that can be applied to F_2, so that F_2 coincides with F_1, according to equation (3.9):

$${}^1T_2(F_1, F_2) = (T_1 : T_2^{-1}) \tag{3.13}$$

The notation $(T_1 : T_2)$ will further be used to illustrate homogeneous matrix multiplication of two frames.

3.2.3 Coordinate systems

KRL uses a set of previously defined Cartesian coordinate systems, which represent common coordinate systems used in robotics. Their relationship is shown in figure 3.6 and their applications are explained below.

World
The world coordinate system is permanently defined and serves as a main coordinate system for the robot. It is set during commissioning and can not be changed. It is also used to calibrate and measure a robot before initial operation.

Robroot
Robroot is always located at the robot's base and defines the position of the robot relative to the world coordinate system. Changing the robot's root position (e.g. with an external linear axis) is often necessary to improve reachability and change axis positions of the robot to avoid collisions. Moving the robot on an external linear axis, also moves the robroot frame. Thus, robroot is commonly used to calculate the inverse kinematics of the robot, which are only dependent on the joints and links of the robot from this frame. Additionally, it is particularly useful to determine the work envelope of a robot and position two or more robots relative to each other.

Base
The base coordinate systems serves as a basis for the robot's motion programming. Every motion of the robot is performed relative to the current base coordinate system. The base can be a work-piece, a table or anything with known geometric relationships to the working environment. It is common practice to change the base during a robot program, especially for

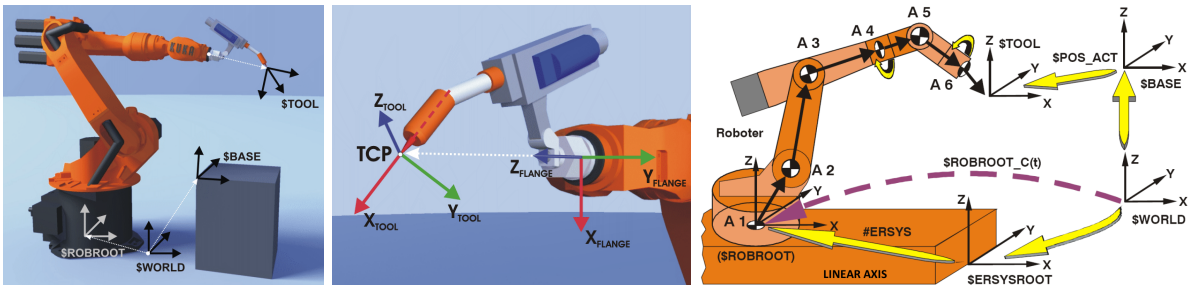

Figure 3.6: Overview of robot coordinate systems (left), Tool, TCP and flange relationship (center) and linkage of coordinate systems (right). [12]

large work-pieces, since the greater the distance to the base, the greater the influence of angular deviations on the position of the tool tip becomes.
Commonly, a base needs to be measured and calibrated since its exact position and orientation is not known priorly, but can sometimes be retrieved from CAD. Precision is crucial here, since small deviations lead to inaccurate motion and unpredictable behavior of the robot.

Flange

In general, finding the position and orientation of the end-point of a robot relative to the robot's base is called the forward kinematics problem. It is solved by taking the values of all axis joints and link parameters of the robot into account and calculating the transformations between them. This results in a 6D pose, which can be described by a frame attached to the end-point of the last axis link of the robot (flange center point) and serves as the origin of the flange coordinate system. Its orientation is commonly defined by the Denavit-Hartenberg convention. [10]

Tool

The tool coordinate system (TCS) is used to define any mechanical structure attached to the robot flange, such as robotic grippers, manipulators or arc welding guns. The origin of the tool coordinate system is called the tool center point (TCP). The TCP can be thought of as the working point of the robot and is the point in relation to which all robot positioning is defined. For certain tools the TCP is positioned at the tool tip (as shown in figure 3.6) and can be calibrated. However, it is also common to use metrics taken directly from CAD. Changing the TCP during a robot program is also possible. It allows to execute motions which would otherwise be difficult to perform (e.g. certain rotary motions), or work with adjustable end-effectors which by its nature require non-fixed TCPs.

Actual robot pose

In KRL, a special frame is introduced that always expresses the position and orientation of the actual TCP in its current base. It is used to program motions relative to the base coordinate system, and can in most cases be thought of as the actual pose of the robot. In KRL it is called *pos_act*.

Changing the coordinate system, or expressing a frame in a different coordinate system is easily achieved by the geometric operator. In KRL all coordinate systems are linked, as depicted in figure 3.6 (right). For example, the actual TCP position of the robot in its world coordinate system can be calculated as follows:

$$T_{\mathrm{TCP}} = (T_{\mathrm{BASE}} : T_{\mathrm{POS\_ACT}}) \tag{3.14}$$

3.2.4 Motion programming

In general, robots can be programmed by two types of motion commands: Point-to-point (PTP) and continuous path (CP) motions.

Point-to-point
A PTP motions moves the TCP from a start point to a target point on the time-wise fastest path possible. The robot calculates the difference in axis angles between both points. The result is a path that is not a straight line, since the robot's axes are rotational, but most likely a curved path. Thus, the TCP will unpredictably deviate from a straight line. Also the orientation of the tool may change during a PTP motion. An example of a PTP motion is shown in figure 3.7 (left).

Continuous path
CP-motion commands are used to guide the TCP along a previously defined path. The tool orientation can be specified to remain unchanged during the motion, or reach a final orientation at the end of the path. CP-motions can also be used to perform solely rotational movements about a fixed TCP.
KUKA robots can be programmed by two basic types of continuous motion commands: Linear (LIN) and circular (CIRC) motions, as depicted in figure 3.7. Also, spline commands for more complex curved paths are available.

All motion types can also be approximated, so that the end point of a motion command is not exactly reached, but the path is altered to move to the succeeding point on a shorter path. This enables the robot to guide the TCP along a path faster without slowing down and stopping at each end point in the command chain.

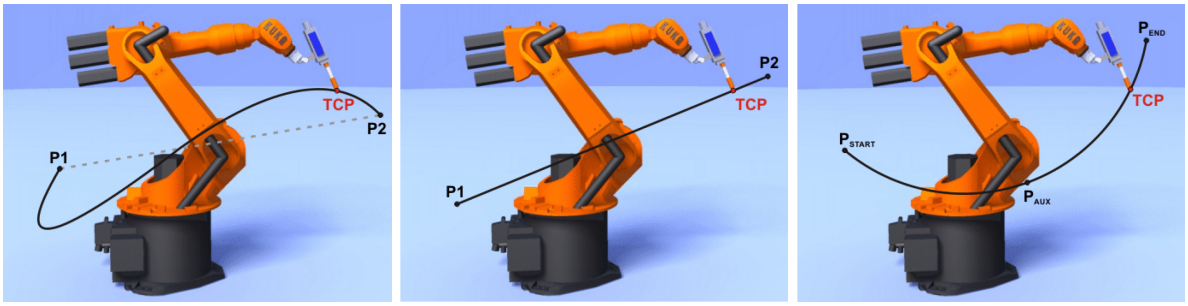

Figure 3.7: Basic principles of motion programming: Point-To-Point (left), Linear (center), circular (right). [12]

Chapter 4

Implementation

The following chapter explains the functional principle behind the adjusting process and highlights the conceptual design of the robot program. Additionally, the calculation of set-angles for each element of the robotic end-effector derived from CAD is shown. Further, it presents the integration of the adjusting station into the robot cell and shows how each robot is able to actuate the components of the adjusting station.

4.1 Functional principle

An overview of the measuring and adjusting process is given in figure 4.1 and is used as a basis for the following section.
The adjusting station was originally split up in two parts, thus the whole process can be thought of as two sub-processes: One for measuring, and one for adjusting each element. The process always starts at the innermost element of each end-effector side, and is applied consecutively for each of the following elements. This way, the position and orientation of each element is traceable, since every element is affected by the ball joint orientation of its predecessors. Once the first side of the end-effector is adjusted, the end-effector is rotated 180° about the Z-axis of the robot's flange coordinate system and the adjusting algorithm is applied to the other side in the same way. The rotation is necessary for reasons of collision and the design of the end-effector. Firstly, due to the fact that the downward-facing sensor is tilted, measurements can only be executed from one side without colliding with the sensor mounting arm. Secondly, all elements on both sides are manufactured equally, thus the tightening spindle can only be attached from one side to the ball joint mount and loosen the joint.

The main purpose of the measuring process is to serve as a target-performance comparison and align each element parallel to the base coordinate system. Thus, it serves as a preparatory step, in order to align the orientation of each element to the clamping position of the adjusting station, which allows it to be processed in the adjusting process. This is achieved by the two retro-reflective sensors, which measure the tube structure of each element. Every angular deviation is determined separately for each axis. The angular deviation is used to align the element parallel to the base coordinate system, by a rotary motion about one axis only. As

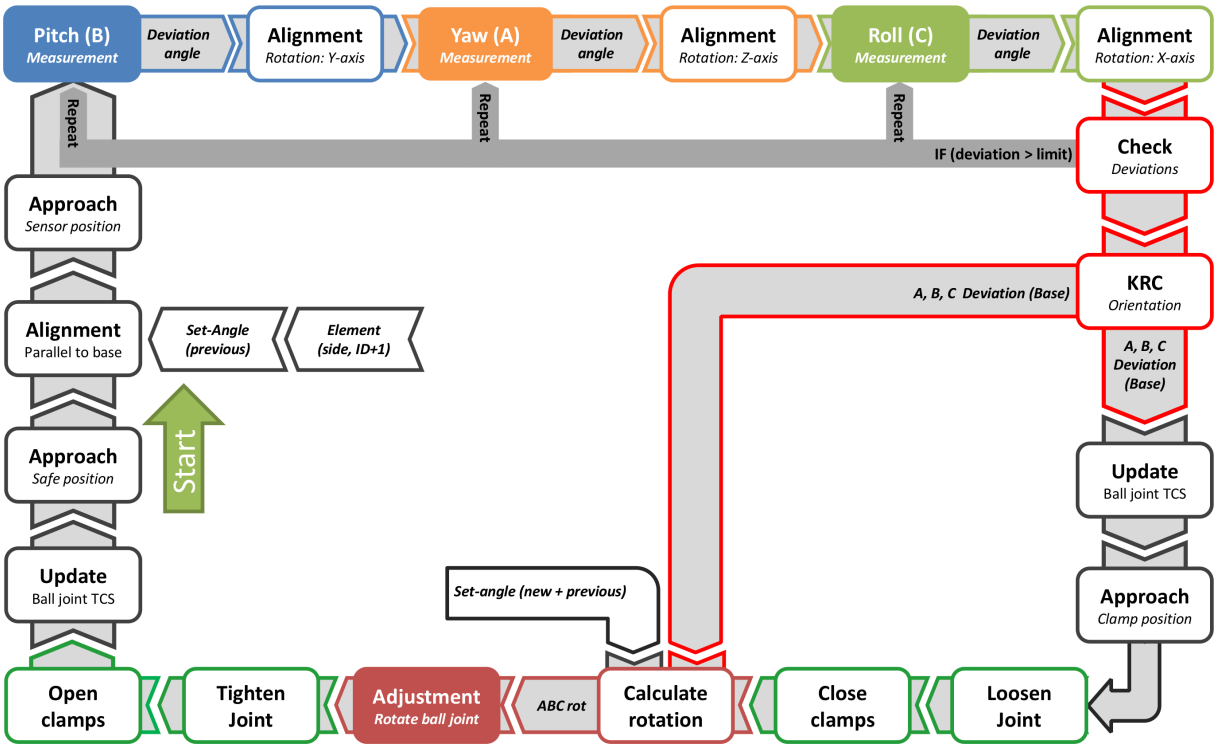

Figure 4.1: Process overview of measurement and adjusting cycle for a single element.

a consequence, the element should be fully aligned to the base coordinate system after three angular deviation measurements (one for each axis). Once an element is fully aligned, its precise orientation can be obtained from the KRC. However, this is only possible due to a special choice of the tool coordinate system, as described in the next section 4.1.1. The advantage of this approach is, that the measured angles can be disregarded and do not need to be used to update the orientation of the element after each rotation. Additionally, this should avoid integrating small angular errors between the measured deviation angles and the orientation the KRC provides after the alignment, and thus result in a more accurate process. The measurement process is described in more detail in section 4.1.2.

Once the measuring process is finished, the element is aligned to the base of the adjusting station, so that the adjusting cycle can be processed. At first, the element needs to be moved to the clamping position without changing its orientation. In this position, the ball joint is loosened and two clamping jaws fix the element in place. Then, the robot is used to adjust the orientation of the joint by performing a solely rotary motion about the center of the ball joint. Afterwards, the joint is tightened and the clamps are opened, so the element that has been rotated can be lifted out of the clamping position. Finally, the measuring process can start over for the next element in the chain. The adjusting process is further described in section 4.1.3.

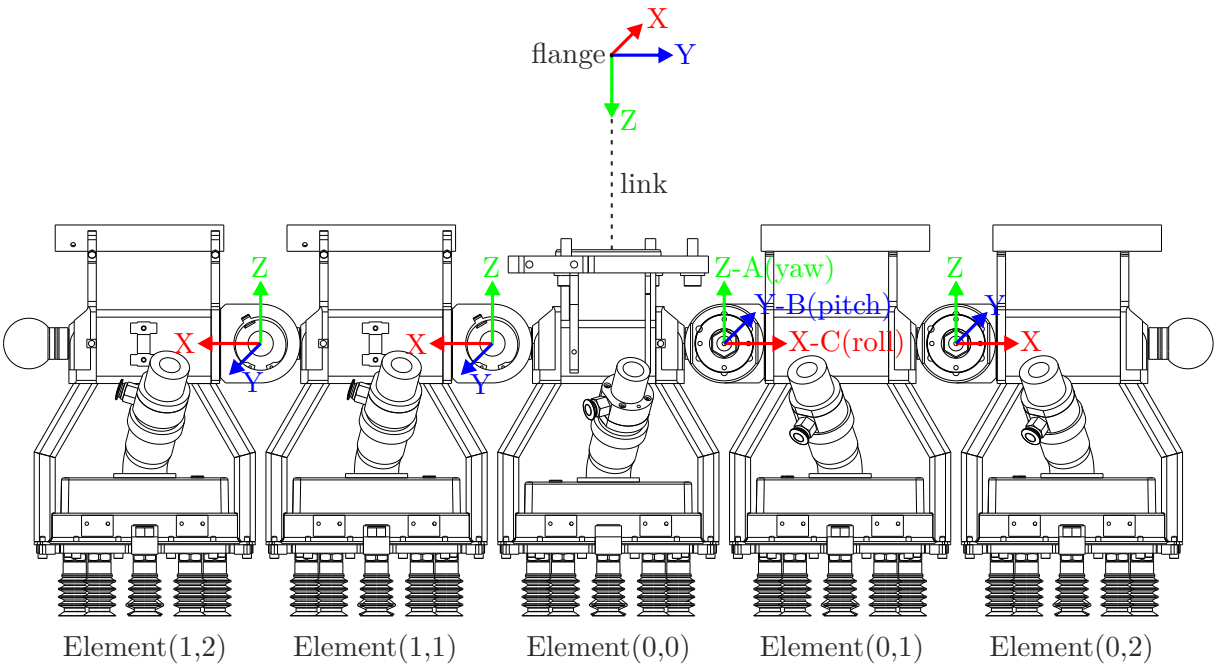

Figure 4.2: TCP definition for each element and relationship between the flange and end-effector coordinate systems.

4.1.1 Tool and base definition

For the whole process the origin and orientation of the base is fixed. It is defined by three measuring tips as previously shown in figure 3.4. These measuring tips are used as a reference during base calibration. Due to the requirement, that the adjusting station needs to be mobile and used in different robot cells, every rotation and movement of the robot is programmed in the base coordinate system of the adjusting station.

Particular attention has to be devoted to the location of the TCP, due to its influence on the adjusting process. One logical possibility, from a manufacturing point of view, is to place the TCP at the tip of the central suction cup below each element, since these gripping points are essential during pick and place operations. However, doing so complicates the rotary adjusting motion, during which the ball joint position has to stay fixed at all times, in order to avoid any stress or damage to the mechanical components. A rotary motion that moves the TCP around the ball joint center on a spherical arc with a fixed radius is required, but involves the calculation of a complex continuous path movement (circular or spline) for every rotation. Instead, for the measuring and adjusting process, the TCP was chosen to be in the center of each ball joint. This simplifies the adjusting motion, since the KRC is capable of performing rotations without moving the TCP on its own (linear continuous path motion), as previously described in section 3.2.4.
The orientation of the tool coordinate system was chosen to be parallel with the base. This has advantages to the underlying concept of the measurement process, since the initial orientation

of the KRC (A, B, C) is zero for all angles. Of course, this is only the case if the element is precisely aligned. Thus, every angular deviation can be measured directly and compensated without any transformation during the measurement process.
To achieve this, the tool coordinate system of the robot has to be rotated with respect to the flange coordinate system. As seen in figure 4.2, the TCPs on right-hand side of the end-effector need to be rotated 90° about Z- and 180° about the X-axis, so that both coordinate systems align. The left-hand side is rotated −90° about Z- and 180° about the resulting new X-axis, so that the tool coordinate system is orientated parallel to the base for the left-hand side as well. This results from the fact that the end-effector itself is rotated 180° about the Z-axis after the adjustment of the first side is finished.

In order to keep track of the absolute position and orientation of each element, a new tool coordinate system (TCS) is introduced. Its origin is located at the flange center point, but its orientation is not parallel to the flange coordinate system. Instead, the orientation is chosen to be parallel to the base, which is the same as the ball joint orientation of element(0,1) in its zero position, as seen in figure 4.2. This allows to view the end-effector as a kinematic chain, in which each element is regarded as a link with a fixed length (equal to the joint-to-joint distance) interconnected by a ball joint. Calculation of the next ball joint frame is easily computed by traversing the joint-to-joint distance along the X-axis of the previous element, while taking the orientation of the previous ball joint coordinate system into account. The TCPs of elements(0,1) and (1,1) are always fixed, since they are mechanically attached to the central element(0,0). Thus, they serve as the starting point for the TCP calculations.

In order to work with the rotation angles more intuitively, they are named yaw (A), pitch (B) and roll (C) respectively, as shown in figure 4.2, and are used to describe the measuring process in the following section.

4.1.2 Measuring process

As previously mentioned, the underlying principle of the measuring process is to align each element parallel to the base coordinate system, so it can be processed and moved to the clamping position of the adjusting station. Thus, it serves as a necessary preparation step to compensate for inaccuracies that result from the adjusting process of the previous elements.

The measurement principle can similarly be explained for all angles as follows: Two retro-reflective sensors are used in conjunction with the motion of the robot, to determine the orientation of each element. For that purpose, the robot executes a linear movement along a single axis towards the sensor intersection point. During this operation, a sensor interrupt is triggered if the sensor ray hits the tube structure. This commands the robot to halt. Since each sensor has a scanning range, that can be manually adjusted with a potentiometer, it prevents the sensor from triggering unintentionally if any farther afield object other than the measuring tube is detected. The linear movement is executed several times from pre-positions that are offset from the sensor intersection point ($\overrightarrow{P_{\text{int}}}$). The offsets are described by search length s and measurement width d, as calculated in table 4.1. Here, s describes the maximum search length during which the

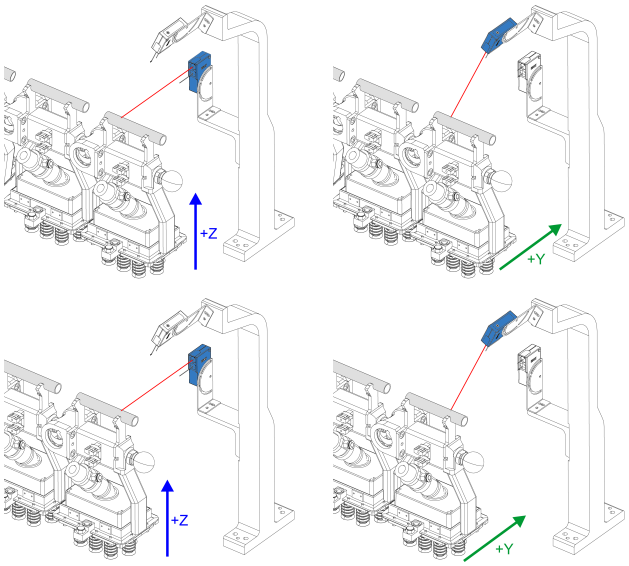

Figure 4.3: Measuring process for pitch (a) and yaw (b).

robot tries to detect an interrupt and d is used to obtain two different measurement points on the tube structure. These are necessary to calculate the angular deviations.
In general, increasing the measurement width d, improves the accuracy of the measurement. This results from the fact, that both measured points are at a greater distance towards each other, thus the angle of the measuring tube can be calculated with higher accuracy. At the same time, this worsens the reliability of the measurement. It becomes less likely for the robot to generate an interrupt, the greater the angular deviation. This behavior can be explained by the effect, that the measurement tube moves out of the sensor detection area for large deviations. However, d is limited by the length of the measuring tube. Thus, it was chosen to be half of the tube length as a trade-off between accuracy and reliability, but can be varied to enhance either of the two.
In case no sensor interrupt occurred, the robot stops automatically after the end of search length s is reached, in order to avoid collision with the adjusting station.

The interrupt positions are used to determine the angular deviation of the element to the base coordinate system. Every deviation angle is determined in separate measurements consecutively. After each successful angle measurement, the angular deviation is compensated by a rotary motion of the robot. That way each element axis is aligned to the base coordinate system one after another.

The measurement for yaw (A) is shown in figure 4.3 b). The robot performs two horizontal linear search movements in positive Y-direction. Therefore, only the vertical sensor must be enabled. The pre-positions are offset in Y by half the search length s, in order to start the

	yaw[1]	yaw[2]	pitch[1]	pitch[2]	roll
X	$X_{\text{int}} - d$	$X_{\text{int}} + d$	$X_{int} - d$	$X_{\text{int}} + d$	X_{int}
Y	$Y_{\text{int}} - \frac{s}{2}$	$Y_{\text{int}} - \frac{s}{2}$	Y_{int}	Y_{int}	$Y_{\text{int}} - \frac{s}{2}$
Z	Z_{int}	Z_{int}	$Z_{\text{int}} - \frac{s}{2}$	$Z_{\text{int}} - \frac{s}{2}$	Z_{int}

Table 4.1: Calculation of pre-positions relative to intersection point $\overrightarrow{P_{\text{int}}}$ with search length s and measurement width d.

search motion next to the sensor intersection point, and are varied by measurement width $\pm d$ along X. The angular deviation in yaw can be calculated from the difference in Y of the two interrupt positions ($\overrightarrow{P_1}$, $\overrightarrow{P_2}$) by the following equation:

$$A = \text{atan2}(\Delta Y, 2d) \tag{4.1}$$

The measurement process for pitch (B) works in a similar manner, as shown in figure 4.3 a). The robot performs two vertical linear search movements in positive Z-direction, so that only the horizontal sensor must be enabled. The pre-positions are offset in Z by half the search length s, in order to start below the sensor intersection point, and are varied by measurement width $\pm d$ along X. The angular deviation in pitch can be calculated from the difference in Z of the two interrupt positions ($\overrightarrow{P_1}$, $\overrightarrow{P_2}$) by the following equation:

$$B = \text{atan2}(\Delta Z, 2d) \tag{4.2}$$

As shown in table 4.1 both pre-positions for yaw and pitch are equally varied by measurement width d in X-direction.

The geometrical assembly of the tube and the sensors do not allow to determine the roll angle (C) with two sensor measurements, instead it has to be retrieved solely from a single measurement and a precisely known reference point. For this purpose, the sensor intersection point is used. However, it is necessary that yaw and pitch are previously aligned. Consequently, the roll angle measurement always has to be executed as the final measurement with the current measurement technique.

Measuring the roll angle is possible from two directions: Both Z- and Y- direction. However, as shown in figure 4.4 (right), the difference between the sensor intersection point and the TCP is significantly larger in Y-, than in Z-direction for small angular deviations. Thus, measuring roll from Y-direction yields a higher accuracy.
For that reason, the measurement for roll (C), as shown in figure 4.4, is obtained by one horizontal linear movement in positive Y-direction. The pre-position is offset in Y by half the search length s to start the movement next to the sensor intersection point, similar to the yaw measurement. Since only one measurement is required, no variation with measurement width d is necessary. The angular deviation in yaw can be calculated from the difference in Y of the interrupt position ($\overrightarrow{P_1}$), the sensor intersection point ($\overrightarrow{P_{\text{int}}}$) and TCP to tube distance h by the following equation:

$$C = 90° - \arccos(\frac{Y_{\text{int}} - Y_1}{h}) \tag{4.3}$$

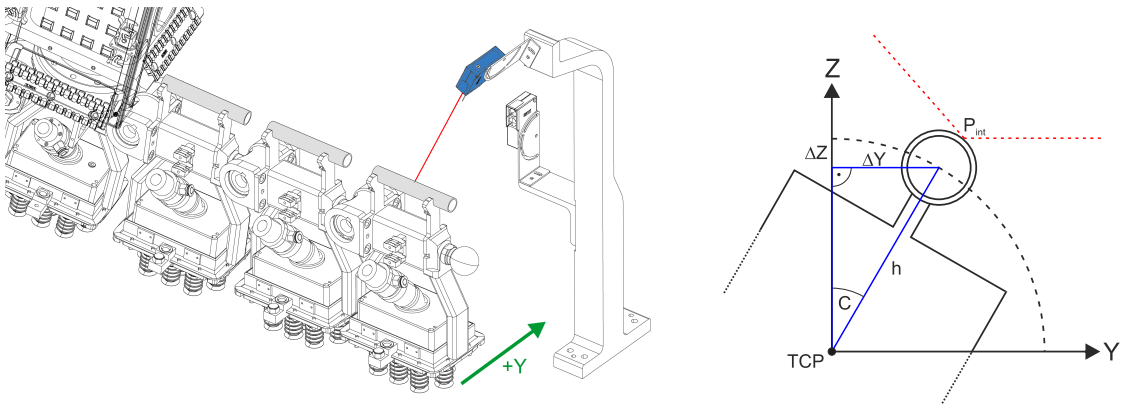

Figure 4.4: Roll measurement principle - Search movement direction (left), calculation of deviation angle (right) with TCP to tube distance h, sensor intersection point P_{int} and angular deviation C.

The angle measurements obtained during the measurement process are not Euler angles in KUKA convention, since the absolute deviation angle to the base is measured every time. In order to measure the angles directly and satisfy KUKA's ZYX convention with intrinsic rotations, measurements of each angle in reverse order would be required. Thus, first measuring roll (X-axis, C), secondly pitch (Y-axis, B) and finally yaw (Z-axis, A). However, as previously mentioned, measuring the roll angle first is not possible with the current measurement technique, since it requires yaw and pitch to be previously aligned. As a consequence, the measured angles would have to be converted to the required Euler convention every time.
To circumvent this, the angle measurements are solely used to align each element parallel to base during the measurement process. The final orientation and deviation angles in KUKA's Euler convention can then be obtained by the KRC after the measuring process is finished and the element is aligned.

The measurement process is repeated if one of the deviation angles exceeds a fixed limit, here the limit was arbitrarily set to 0.5°. It can be adopted to the required accuracy during the measuring process, which has yet to be determined experimentally. This limit is necessary, because a large rotary compensation motion in one axis can result in small deviations for the other axes, especially if the calculated TCP does not precisely coincide with the actual TCP inside the ball joint. This is more likely for the outer elements. Thus, the inaccuracies of the TCPs have a direct impact on the rotation accuracy. As a consequence, a desired rotary motion about a single axis becomes impractical, which leads to an inaccurate alignment. Additionally, the roll angle has to be re-measured every time pitch or yaw are corrected, due to the fact that both angles directly influence the position of the measurement tube, and as a consequence the measured roll angle. The order for measuring yaw and pitch can be changed, however measuring pitch first has shown to be advantageous due to geometrical constraints between the end-effector and the adjusting station. Thus, for unexpected large deviations (e.g. after the end-effector was reset or changed manually), collisions become less likely. Also, less measuring iterations are required.

In order to align each element axis, first the rotary motion has to be calculated. Since the deviation angles are measured in the base coordinate system, the rotary aligning motion also has to be executed in the base, without translating the TCP, in order to avoid collision. However, calculating a rotation in the base coordinate system results in a translation of the TCP, unless it is located at the origin of the base coordinate system. Thus, the rotated target frame needs to be calculated by a transformation with the help of the geometric-operator. It has to be translated back after the transformation in order to make sure that the TCP stays fixed. The target frame is calculated by the following equation, where the rotation frame $F_{\text{rot}} = (0, 0, 0, A, B, C)$ contains one of the measured deviation angles and F_{pos_act} is the current pose of the robot:

$$\begin{aligned} F_{\text{target}} &= (F_{\text{rot}} : F_{pos\_act}) \\ F_{\text{target}}.X &= F_{pos\_act}.X \\ F_{\text{target}}.Y &= F_{pos\_act}.Y \\ F_{\text{target}}.Z &= F_{pos\_act}.Z \end{aligned} \tag{4.4}$$

The target frame then contains the new orientation and is approached by the robot with a solely rotary motion that aligns one of the element axis parallel to the base coordinate system. After all axes are measured and aligned, the current orientation of the robot is saved in $F_{\Delta\varphi}$ and used to update the orientation of the TCP (ball joint) accordingly. Afterwards, the robot proceeds to the adjusting station without changing its orientation.

4.1.3 Adjusting process

The following section describes the adjustment of a single element in detail by following the chronological sequence of the adjusting process.
Before the robot is allowed to lower an element into the clamping position, a security check is performed, to ensure that the clamps are open and the tightening spindle is detached, in order to prevent collision. As previously described in section 3.1.3, two guiding pins help to align the element onto the support surface. However, the pins have a loose fit, in order to tolerate inaccuracies resulting from an imprecise TCP or deviations during the measurement process.
Before the clamps are closed and the element is fixed in place, the ball joint connection has to be loosened by the tightening spindle. This is necessary, because closing the clamps will force the element into the clamping position. During this, the element may still move slightly. Therefore, loosening the joint priorly decreases mechanical stress on the joint and prevents it from wearing out.

In this state, a rotation can be performed about the TCP by the robot to adjust the ball joint's orientation for all three axis simultaneously. To calculate the required rotation, that takes the measured deviations from the expected element position into account, the desired set-angles have to be transformed. These transformations are derived from the two-dimensional case, as shown figure 4.5.
The general idea of the adjusting process is to adjust an element to its new orientation (F_{new}), as described by the set-angles β. Further, it needs to be able to deal with adjustments performed in previous cycles. Thus, the set-angles of the previous adjustment α have to be known. The

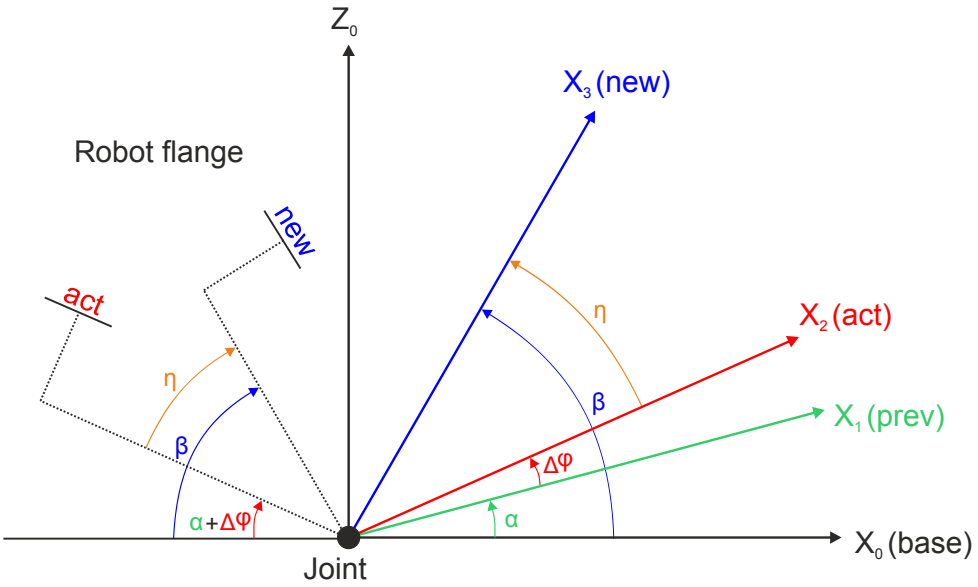

Figure 4.5: 2D overview of the adjusting process to calculate the transformation to the new set-angle orientation. Internal coordinate system (right-hand side of coordinate system), rotation and translation the robot flange hast to perform (left-hand side of coordinate system).

previous orientation F_{prev} can also be thought of as the expected orientation, which is corrected by the angular deviations $\Delta\varphi$ obtained during the measuring process. The orientation after the measuring process is the actual orientation (F_{act}) of the ball joint.
With this information, we can obtain the required rotation η from the actual ball joint orientation to the new orientation, which is described by the transformation matrix ${}^3T_2$, calculated by pre-multiplying the following transformation matrices as follows:

$$ {}^3T_2 = {}^3T_0 \cdot {}^0T_1 \cdot {}^1T_2 \tag{4.5} $$

Here, ${}^1T_2$ is the inverse of the deviation angles determined in the measuring process, ${}^0T_1$ is the inverse of the previous set-angle orientation and ${}^3T_0$ describes the new set-angle orientation.
This corresponds to the following operations in KRL with the geometric operator:

$$ \begin{aligned} F_{\text{rot}} &= (F_{\text{new}} : F_{prev}^{-1}) \\ F_{\text{rot}} &= {F_{\text{rot}}}^{-1} \\ F_{\text{rot}} &= (F_{\text{rot}} : F_{\Delta\varphi}^{-1}) \\ F_{\text{target}} &= (F_{\text{rot}} : F_{pos\_act}) \\ F_{\text{target}}.XYZ &= F_{pos\_act}.XYZ \end{aligned} \tag{4.6} $$

It should be noted, that the rotation the robot has to perform is executed into the opposite rotation direction, as shown by the direction of η in figure 4.5 (left). As a consequence, the calculated rotation F_{rot} is inverted.
Since the measured deviation of the measuring process $F_{\Delta\varphi}$ was determined in the robot flange

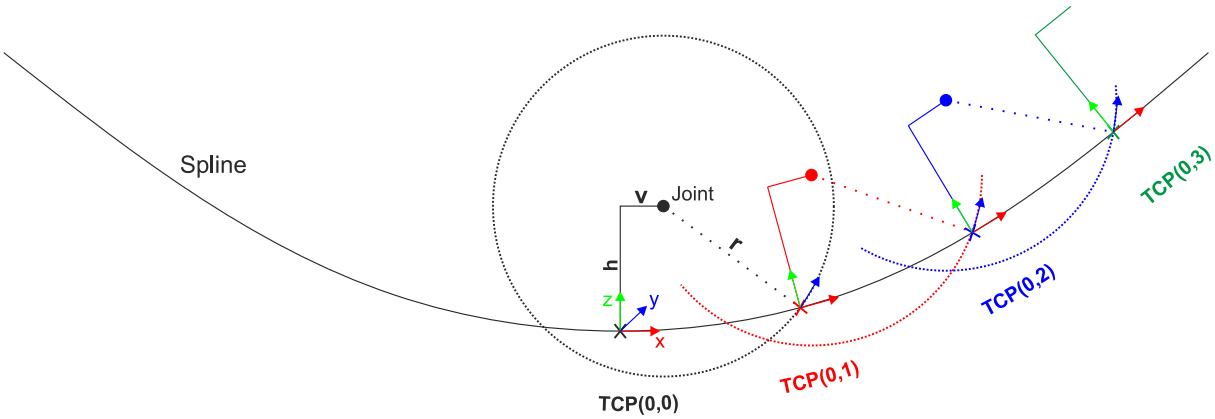

Figure 4.6: Set-angle determination (2D) for right-hand side of the end-effector visualizing the geometrical principle.

coordinate system, it is already inverted and should not be inverted twice, thus only F_{rot} is inverted. The target frame (F_{target}) then contains the new orientation and describes a solely rotary motion about the TCP. It can be executed with the element held in place by the clamps. The rotation direction correlates to the coordinate system shown in figure 4.2. The position of the target frame is overwritten with the position of the actual pose (F_{pos_act}), to avoid a translatory movement of the TCP. However, it is important that a linear CP-motion command is used, instead of a PTP motion command. A PTP motion could potentially change the TCP's position during rotation, since it directly controls the joints of the robot only, and does not consider the path of the TCP.
The target frame is also used to update the TCS for that element in order to store its new orientation. Afterwards, the joint is tightened, so the clamps can be loosened and the element is moved out of the adjusting station.

4.2 Set-angle determination

The set-angles for each joint are directly calculated from CAD. For this purpose, the 3D robot-modeling software Dassault Systemes Delmia V5 [24] based on CATIA is used, which offers a macro extension called *CATvba*. With this macro extension it is possible to control all functions and operations that can be performed in the CAD program, such as geometrical operations. The underlying script language is Visual Basic. The determination of set-angles is described geometrically in the following section.

The general idea is to match the shape of the end-effector to a 3D-spline that is derived from the surface geometry of the mold, in which the carbon fiber layers will be placed down by the robot. For that to work, the ball joints of all elements have to be adjusted, so that the gripping-points (central suction cup below each element, see figure 4.7) touch the surface of the mold.

A two-dimensional simplification of the set-angle determination is shown in figure 4.6 for the

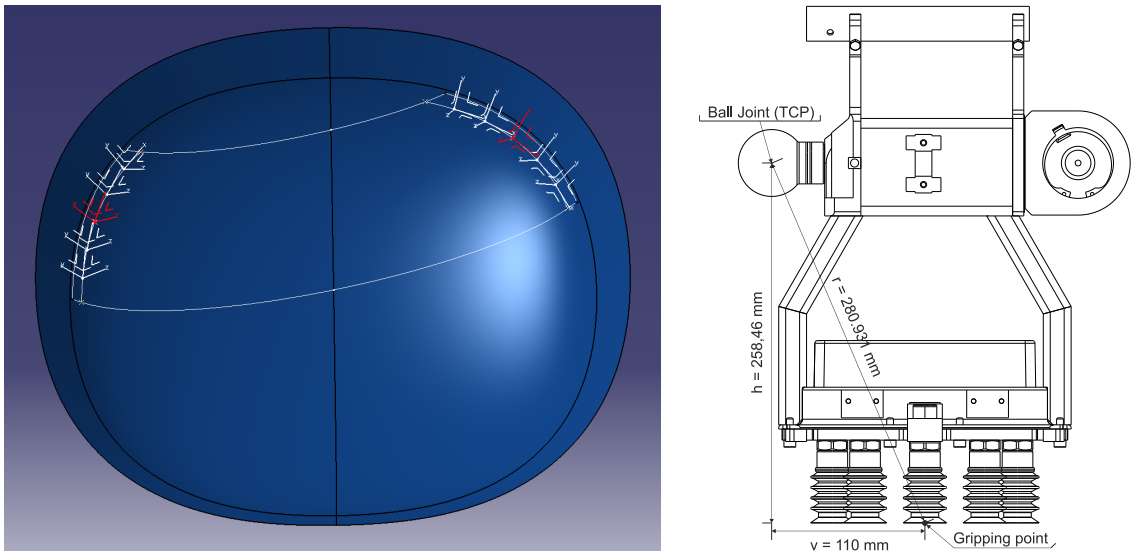

Figure 4.7: Extracted spline on preform in Delmia with calculated gripping-point coordinate systems (left) and technical drawing of an element with required dimensions (right).

right-hand side of the end-effector. Here, the gripping-point of the central element is positioned in the center of the spline. A coordinate system is defined, where the positive Z axis points perpendicular to the inner side of the spline (surface normal in 3D), and the positive X axis points tangent to the spline at this point. To find the position of the next gripping-point in this coordinate system, first the ball joint position has to be determined. Since the gripping-point and the ball joint of the same element are always fixed to each other, a simple translation by h along the Z-axis and v along the X-axis is sufficient. Here, h is the fixed height form the gripping-point to the ball joint along Z, and v is the fixed vertical length from the gripping point to the ball joint (see figure 4.7 as a reference), which are the same for all elements.
Rotating about the ball joint effectively moves the gripping-point of the next element on a circle (sphere in 3D) with a fixed radius r, which is used to determine the next gripping-point. Since the circle and the spline intersect two times, the farther afield intersection from the central element determines the gripping point of the next element. At this point, a new coordinate system is defined by the same rules that applied to the central element. From here on, the process can be repeated for the remaining elements on that side and works similarly for the left-hand side of the end-effector.
The resulting coordinate systems are then used to determine the set-angles for each element. The orientation of the coordinate system at the first gripping-point has to be determined in the coordinate system of the central gripping-point. Iteratively speaking, the coordinate system at a gripping-point always has to be expressed in the coordinate system of the preceding element, which is achieved by a change of basis. This yields the required change of orientation between two consecutive elements. It can be expressed as rotation matrix, from which the set-angles for each element can be determined (see equation (3.4)).
The *CATvba*-script was designed dynamically to deal with arbitrary numbers of elements per side, so that different shapes and sizes of cut fiber layers and preforms can be processed.

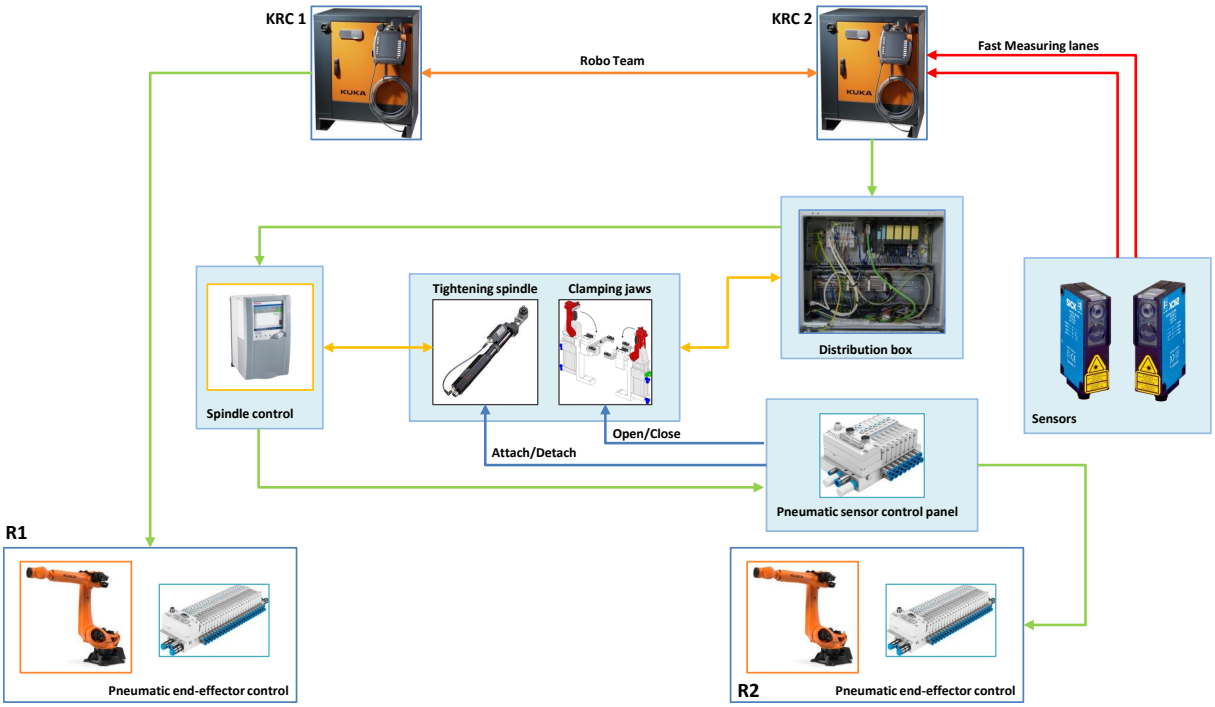

Figure 4.8: Simplified schematic of electrical and pneumatic connections, with EtherCAT (green), pneumatic pressure (blue), sensor values (yellow), fast measuring lanes (red) and RoboTeam communication (orange).

4.3 Electrical and mechanical controlling

The components of the adjusting station are connected via EtherCAT [3]. EtherCAT is an ethernet-based fieldbus system that uses a master-slave networking protocol and is suitable for hard and soft real-time application. Its functional principle can be explained by the way the protocols treats the standard Ethernet packages (according to IEEE 802.3). Instead of receiving, interpreting and copying the data at every node, an EtherCAT slave reads the data addressed to it at all times, while the data stream passes through the devices. Thus, data can be read from and inserted into the data stream 'on the fly'. However, this requires all networking devices to be configured and known in the right order priorly.

In its current configuration, each KRC in the robot cell is configured as a master, which controls all devices in the networking chain. However, two masters can not be connected to the same network without additional hardware (master-master bridge). Because of that, only one of the robots can be connected to the adjusting station and control its components. As shown in the schematic overview of the connections given in figure 4.8, only R2 is connected to the adjusting station. However, both robots need to be able to control the I/Os of the adjusting station. A solution was derived from the property that both robots are already configured as a RoboTeam [13], since they have to cooperatively perform pick and place operations. The RoboTeam configuration allows robots to synchronize their motion commands. Also, it offers

the possibility to remotely execute instructions on another robot, which allows R1 to control the I/Os of R2.

The configuration of the EtherCAT chain is done in KUKA.WorkVisual [14] an integrated development environment (IDE) used for programming and configuring KUKA robots. Each robot has a total of 4096 inputs and outputs that can be setup according to the deployed hardware that is connected to the robot. The I/Os were configured based on the documentation of the electrical circuit diagrams of the robot cell and the adjusting station. An overview of the I/O configuration is given in Appendix A.2.

The sensors for measuring the orientation of each element are not connected via EtherCAT. Instead, they use two of the four prioritized inputs on the KRC, called fast measuring inputs. Both require an additional dedicated cable to be connected to the KRC directly, as shown in figure 4.8. Thus, the outputs of the sensors are directly wired to the KRC and solely transmit an analog signal (high/low). Thus, the fast measuring lanes offer a lower latency compared to EtherCAT and should result in more precise measurements, while at the same time removing the signal latency as a potential bottle-neck.

Mechanical controlling of the clamping jaws, the vacuum grippers and the wrench arm that attaches the tightening spindle are all controlled pneumatically. Pneumatic valves, which are controlled electronically and are connected to the EtherCAT chain, can be actuated to result in the desired state. Additional sensors monitor the state of the valves and are also read out via the EtherCAT bus.

A spindle control system from Bosch/Rexroth is deployed and used to open or loosen the ball joint connection. Loosening and tightening torque is specified ($150\,\mathrm{N \cdot m}$) and a clock-wise or counter clock-wise screw command can be sent via EtherCAT. Also, the state of the screw cycle can be monitored, to ensure that the ball joint is tightened or loosened after the screw cycle is finished. A control diagram of the tightening spindle is shown in figure A.1.

Chapter 5

Evaluation

The following chapter describes the evaluation process and the experiments, that were conducted to test the functionality of the adjusting system. Additionally, it highlights the current hardware state of the adjusting station and describes software solutions that were utilized to circumvent some of the current hardware deficiencies.

5.1 Hardware deficiencies

The following chapter has to be evaluated with respect to the current hardware state of the end-effector, which is still in its testing phase. During the evaluation, the following hardware deficiencies could be observed:
Firstly, attrition of the threaded ball joint heads caused dowel pins and holes that align each thread to be worn out. As a consequence, the joints are not fully fixed and can still move to a small degree, even if the ball joints are tightened properly.
Further, the tightening spindle was not operable, probably due to a faulty conduit between the control system and EC motor, as depicted in figure A.2. As consequence, every screwing had to be performed manually with a torque wrench to loosen and tighten the ball joints. The lever arm of the torque wrench additionally applies a translatory force to the element during clamping, which may cause a shift in position of the element.

The experiments showed, that the tube structures to measure the orientation of each element, are slightly offset (angular and translatory) and do not exactly correlate to the bottom surface of each element. This is presumably caused by thermal warpage of the welded parts during manufacturing and was not thought of during the design stage of the end-effector. This causes inaccuracies throughout the process, since the alignment during the measuring process does not exactly fit to the support surface of the clamping position. Especially, the translatory offset emerged to be a challenge for the roll angle measurement, since it relies on a single measurement and the distance to a fixed reference point (sensor intersection point). Theoretically, the ideal sensor intersection point can be determined in CAD. However, the sensor intersection point (at which both rays intersect) is not the same point at which the sensor interrupt is triggered (tube hit by the sensor ray). As a consequence, reliable measurements could not be obtained with a

fixed sensor intersection point, thus a software solution that calibrates each element was used to correct the hardware state and is explained in the following section.
Furthermore, an additional measurement was implemented, that measures each element after the adjustment process to compensate inaccurate set-angles, which falsely influence the TCP of the following element. However, with regard to process time and the final program cycle, this measurement should be avoided, if hardware upgrades proof a similar result in accuracy.
Due to these deficiencies, the final accuracy of the adjusting process can not be determined at the current state. However, the basic functionality of the developed robot program can be validated within the limits of the hardware and potentially erroneous influences that additionally affect the accuracy of the process can be shown.

5.1.1 Initial operation and calibration

The process cycle depends on two points, which are essential for the accuracy of the measurement and adjusting process: The clamping position and the sensor intersection point.
Determining the clamping position is done manually. The position has to fit to the support surface (z-value), the guiding pins, the clamping jaws and the tightening spindle (x- and y-value). For that purpose, the element is positioned approximately on the support surface and its position is varied manually to satisfy all hardware components. The position of the guiding pins is movable, and the clamping jaws pins can be adjusted by leveling shims to correct any discrepancy in their alignment as well.

The sensor intersection point is determined by a calibration program. As a precondition, the ball joint of the element that is to be calibrated has to be adjusted to its initial state (set-angles set to 0). This can be achieved manually by a set-plate that matches the bottom surfaces of two consecutive elements parallel to each other (see figure A.3 for reference). Thus, the central element, that is rigidly fixed to the robot flange, can be used to align the innermost elements on each end-effector side.
The calibration program uses the linear search movements of the measuring process to take 30 measurements of the tube structure without varying the starting position. This way, the sensor intersection point can be estimated by the mean of the measurement positions, that is finally used as a reference point for measuring the roll angle. This compensates the hardware inaccuracies and allows an adequate measurement of the roll angle. So far, only the innermost elements of each end-effector side are calibrated, since only these elements can be aligned reproducibly with the fixed center element of the end-effector. The accuracy of the calibration process is evaluated in section 5.2.1.
It should be noted, that the initial operation and calibration process has to be executed for both robots (R1 and R2) separately, due to the fact that the base of the adjusting station is calibrated manually. Base calibration is executed with a measuring tip attached to the central element of each end-effector, in conjunction with the measuring tips of the adjusting station. This is a standard procedure in robotics, although it bears potential inaccuracies in itself. Therefore, displacements between the two base measurements are unavoidable, since manual base calibration is prone to errors. Automated base calibration is possible and planned for future use cases, but is not implemented at this stage.

5.2 Experiments

The following section is used to show the operative readiness of the system and demonstrates the accuracy of the angular measurements and the adjusting process. Several experiments were conducted to test the functionality of the system. At first, the calibration process is evaluated, with respect to the repeatability of the sensor measurements. In an additional experiment, the influence of the TCP velocity on the measuring process is presented, and also the accuracy of the sensors are assessed. Furthermore, experiments were conducted to evaluate the accuracy of measurement and the adjusting process. Finally, both robots were adjusted automatically and used to cooperatively pick and place a layer of carbon fabric to show the functional state of the adjusting process in a practical application.

5.2.1 Accuracy of calibration

In order to determine the accuracy of the calibration, the measurements obtained during the calibration itself can be used. As a preparatory step, the bottom surfaces of the innermost elements on each end-effector side have to be manually aligned to the fixed center element of the end-effector. Before experimental data is gathered, the remaining angular deviation of the innermost element is measured for the pitch and yaw angle and the element is aligned accordingly. In this state, the element is oriented parallel to the base. 30 measurements of the sensor intersection point are obtained by moving the center of the measuring tube towards the sensor intersection point along a single axis of the base coordinate system until an interrupt occurs. After a single measurement, the TCP is moved back to the same starting position, without changing the orientation of the element and the measurement is repeated. For this experiment, robot R1 is used to acquire measurements for both innermost elements of each end-effector side in Y- and in Z-direction. A comparison is shown figure 5.1.

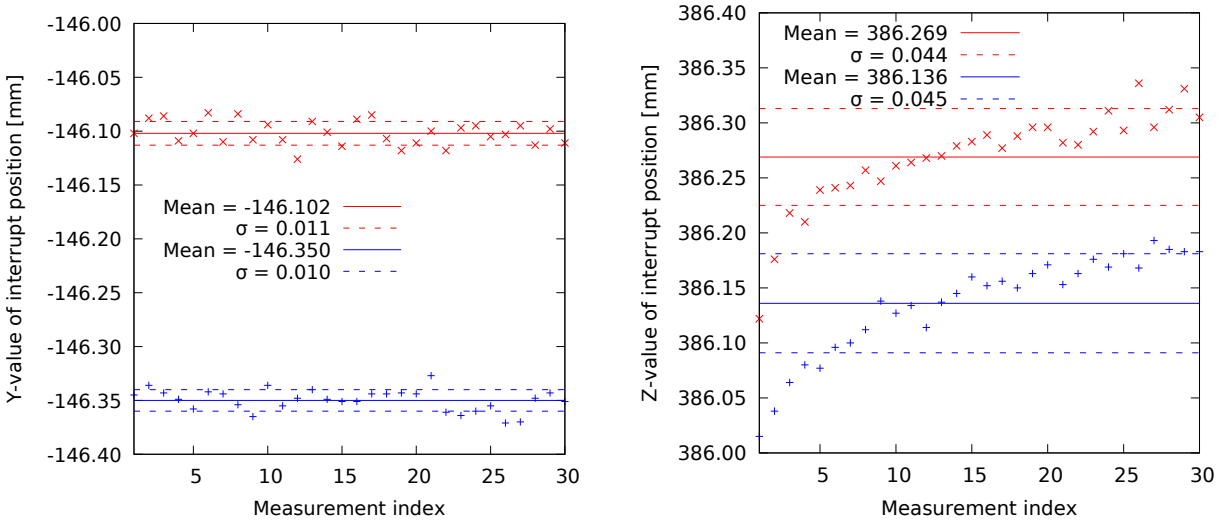

Figure 5.1: Accuracy of calibration for Y-axis (left) and Z-axis (right), comparing element(0,1) (blue) to element(1,1) (red).

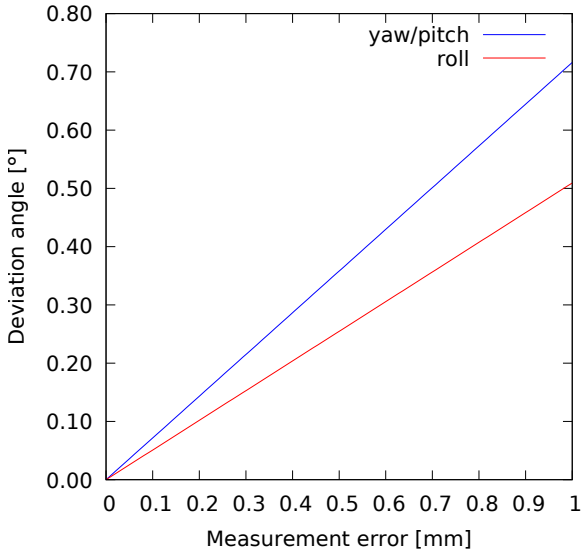

Figure 5.2: Dependency of the deviation angle on the measurement error derived from the mathematical equations as shown for small errors for roll, pitch and yaw.

The data suggests, that the calibration method can be used to determine the sensor intersection point. It should be noted, that only the Y-axis calibration is necessary to accurately calculate the roll angle, which is the purpose of the calibration. As seen in figure 5.1 (left), the distribution of the measurement data for the Y-axis shows little dispersion, as described by the standard deviation of $\sigma = \pm 0.01\,\text{mm}$.
Furthermore, the data shows the large discrepancy between the measurements for the elements on opposite sites of the end-effector. Both element should be ideally alligned, thus result in the same intersection point. However, the difference of 0.248 mm between the intersection value for Y of both sides of the end-effector shows the inaccuracies of the hardware state. As seen in figure 5.2 a measurement discrepancy of 0.248 mm would result in an angular deviation of approximately 0.13° for the roll angle measurement. This shows, that a calibration for both sides is necessary.

The reference of the Z-value of the sensor intersection point is not required to determine the angular deviation, since a fix approximation is sufficient. However, it is included to highlight an underlying problem, that also influences the measuring process and shows the difference in accuracy of the horizontal and vertical search movements. As seen in figure 5.1 (right), the measurements (for both sides) are not evenly distributed. Instead, a convergence to a boundary value can be observed, thus the determined mean of the Z-value of the sensor intersection point becomes impractical. It is not evident, what caused this behavior, due to the large number of erroneous influences that have an impact on the measuring process. An important distinction is the different sensor and its position that is used for the Y- and Z-axis measurements respectively, although both sensors should have the same latency. On the other hand, the data suggests, that the vertical movement (along the Z-axis) can not be executed as precisely compared to the

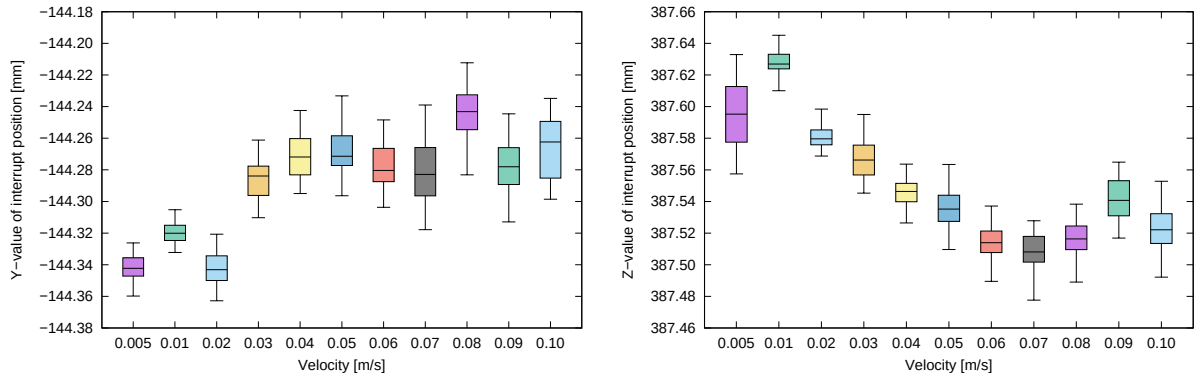

Figure 5.3: Influence of velocity on the measuring process for horizontal measurements in Y-axis direction (left) and vertical measurements in Z-axis direction (right).

horizontal movement (Y-axis). This behavior is presumably caused by gear backlash of the robot's joints during small movements, but could not be fully resolved. As a consequence, the measurement accuracy for pitch, which relies on the Z-axis measurement, is presumably less accurate than the measurement accuracy for yaw and roll, which rely on the Y-axis measurement.

5.2.2 Velocity influence on measuring process

An experiment was conducted to show the influence of the TCP velocity on the measuring process during the linear search movement. For that purpose, the interrupt position of the same object is monitored, similar to the previous experiment. Correspondingly, the linear search motion is executed 30 times from the same starting position. Correspondingly, the velocity of the search motion is varied after 30 measurements, in order to show the influence of velocity on the measuring process. However, the distance of the starting position to the intersection point is decreased, depending on the velocity, in order to decrease the duration of the experiment. The experiment was conducted with robot R2.

The data is shown as boxplots in figure 5.3. It becomes evident, that the interrupt position depends on the velocity that is used during the linear search movement. As a consequence, with increasing velocity, the accuracy of the measuring process decreases. Subsequently, calibration has to be executed with the same speed that is used during the measuring process, in order to determine the accurate sensor interrupt position.
The Y-axis measurements show an increase in dispersion, with increasing velocity. This is expected, since a higher velocity results in a shorter response time for the sensor to trigger an interrupt. Due to the measurement frequency of the sensor, this effect is already observable at low velocities. At the same time, this explains the behavior that the interrupt positions shift towards the position of the sensors, due to the lower response time.
The Z-axis measurements also show a similar position shift. However, dispersion seems to be increasing to a lesser extent with increasing velocity, as shown by smaller boxes compared to the Y-axis data. Except for $v = 0.005\,\mathrm{m\,s^{-1}}$), which presumably results from the fact, that the distance between the starting position and the sensor intersection point was chosen too small.

As a consequence, the influence of gear backlash is potentially greater on this measurement.

Based on this data, the velocity of the linear movements during the measuring process was chosen to be $0.02\,\mathrm{m\,s^{-1}}$ for the following experiments. Dispersion at this velocity is small, while at the same time process time is high. Since the focus of this evaluation lies on accuracy (within hardware limits), a lower velocity was chosen. However, with respect to process time, the velocity could be increased, depending on the desired accuracy throughout the measuring process.

5.2.3 Accuracy of measuring process

In order to determine the accuracy of the measuring process, an experiment was conducted, that measures the orientation of the same element 30 times, by resetting its orientation after each measurement without performing an adjustment. However, it should be noted, that this experiment does not allow to draw a conclusion about the absolute accuracy, but rather about the repeatability of the measuring process. The system itself can not be utilized to determine it's own accuracy, for that purpose independent measurements (e.g. with a laser tracker) would be necessary. However, it can be used to validate the functional principle of the measuring process. The experiment was conducted on robot R1 two times, once for small deviation angles ($< 0.2°$) and once for large deviation angles (4° to 10°).

The measurement accuracy for large deviation angles is shown for each angular measurement in figure 5.4. For that purpose, the element was arbitrarily adjusted. The angular deviation for each angle can be obtained by the mean of the measurements.
By comparing the distribution for each angle, it becomes evident, that the measuring process is capable of reliably determining the angular measurements, even for large deviations. In this case, with a standard deviation of less than $\pm 0.029°$. However, it should be noted, that these measurements were not obtained by a single measurement of each angle. Instead, the measurements were executed twice, according to the functional principle of the measuring process, that a measurement is repeated if its deviation angle too large (current limit: 0.5°).
By analyzing the figures in more detail, the measurement accuracy for roll and yaw is similar, whereas the pitch angle measurement yields larger scattering, which results in a larger standard deviation. This behavior relates to the findings of the first experiment, which showed a larger measurement error for vertical measurements in Z-axis direction.

Figure 5.5 shows the measurement accuracy for small angular deviations. For that purpose, the element was aligned manually in order to measure small deviations. However, the experimental measurement procedure remained the same. It becomes evident, that small deviations ($< 0.2°$) can be accurately compensated by a single measurement. The standard deviation even decreases for yaw and pitch angle measurements, whereas the standard deviation for the roll angle measurement remains the same. Apparently, the measurement error for vertical measurements in Z-axis direction (as suggested by the first experiment) is not significant for small angular deviation. This yields the conclusion, that the obtained inaccuracies for large angular deviations result from the accuracy of the robots joints. Potentially, large rotary motions are performed less accurately.

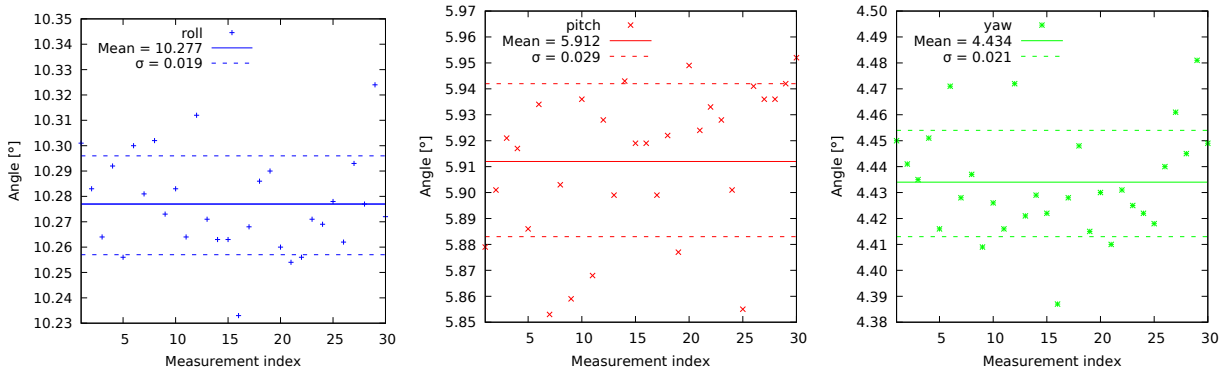

Figure 5.4: Accuracy of the measuring process for roll, pitch and yaw angles of the same element with large angular deviation.

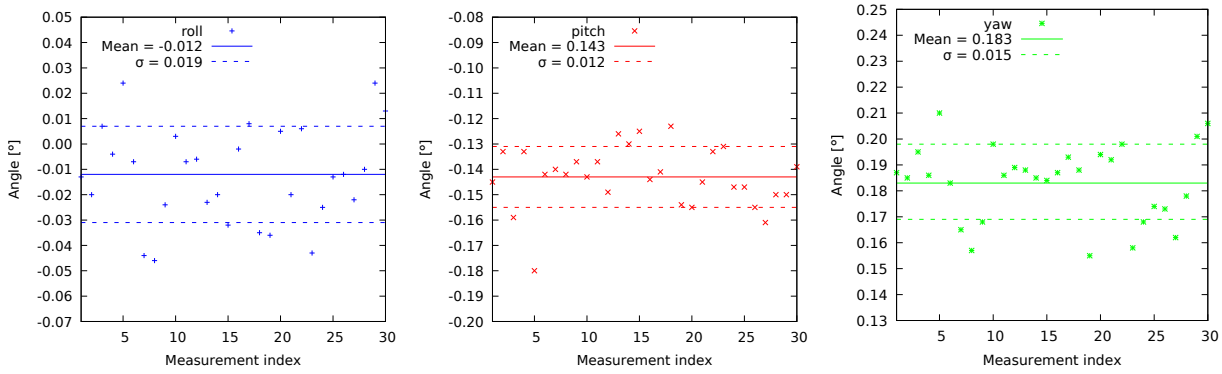

Figure 5.5: Accuracy of the measuring process for roll, pitch and yaw angles of the same element with small angular deviation.

5.2.4 Accuracy of adjusting process

In order to determine the accuracy of the adjusting process, all elements were adjusted from a manually straightened end-effector to the same set-angles by the adjusting process. Subsequently, all tool coordinate systems are reset and the angular deviations are measured by the functional principle of the measuring process for all elements accordingly. The experiment was conducted with robot R1.
However, the measurements do not yield the absolute accuracy of the adjusting process (in degree), as described in section 5.2.3. Instead it can be used to validate the functional principle of the adjusting process. This is achieved by comparing the measured Euler angles after the adjusting process to the set Euler angles. Further, the TCPs calculated from the measured angles is compared to the ideal TCPs calculated from the set Euler angles.

The measured angles and the set-angles are compared in table 5.1 for each element. The data shows an accurate adjustment for all angles (maximum error: $-0.17°$). The similarity of the ranges and the low dispersion suggest, that this is the maximum accuracy that can be measured with the current hardware state. However, the angular deviations are measured by the

functional principle of the measuring process, which by itself has measuring deviations. As a consequence, this negatively impacts the analysis, but still allows to interpret the data, due to the fact, that the measuring deviations are small (see section 5.2.3 for reference).

The data shows, that the yaw angle deviations are larger and most frequent, especially for the left hand side of the end-effector (side one). Thus, the data suggest that not a systematic error of the functional principle is responsible, but presumably hardware inaccuracies cause this behavior.
Further, it was observed, that during clamping the elements shift laterally, since they are only loosely held in place by the guiding pins before clamp-down. The force of the clamping jaws press fit each element into a fixed position, which is responsible for the shift in position of the element. Since the clamping position is determined manually, deviations are expected. This causes inaccuracies in the adjusting process that can not be accounted for. Thus, a re-measurement of the adjusted element was shown to be necessary to improve the accuracy.
At the same time, this behavior presumably causes the frequent measurement deviations for the yaw angle adjustment, since the lateral shift has the greatest influence on the set yaw angle. The support surface has four contact faces, that prevent the fixed element from rotating in roll or pitch direction. Thus, the supporting surface is always parallel to the bottom surface of the element in clamping position. However, a rotation about the Z-axis (yaw) parallel to the support surface is still possible, due to the loose fit of the guiding pins. As a consequence, the lateral shift occurs, when locking the clamping jaws.
Due the fact, that the lateral shift occurs occasionally, not every adjustment is affected in the same way. This yields the conclusion, that inaccuracies in the hardware (e.g. a small angular deviations between the measuring tube and the bottom surface of each element) are responsible for this behavior. Additionally, small deviations in roll and pitch equally contribute to the lateral shift, due to the fact, that the larger the angular deviations, the greater the shift of the element. An additional factor could be the orientation of the support surface and clamping position. If the base and the supporting surface are are not exactly parallel to each other, the elements are always slightly misaligned after the measuring process.
However, improving the hardware state and optimizing the position of the guiding pins and the clamping jaw pins may cause less lateral shift and improve this behavior. As a consequence, the inaccuracies (e.g. angular deviations) in the hardware have to be determined and included into the adjusting process.

Furthermore, the roll angle is the only measurement that is determined by a single sensor measurement, thus hardware inaccuracies should have the greatest impact on the measuring accuracy. Since calibration is only performed for the innermost elements, the measurement accuracy of the outer elements is expected to be worse. However, this effect could not be observed.

TCP comparison
A comparison of the TCPs calculated from the measured angles during the measuring process, compared to the ideal TCPs calculated from the set-angles, is given in table 5.2. The data shows, that the ball joint TCPs can be accurately determined by the process (maximum error:

	Roll (3°)	Δ_{roll}	Pitch (−4°)	Δ_{pitch}	Yaw (5°)	Δ_{yaw}
Element 0-1	3.04	0.04	-3.98	0.02	5.09	0.09
Element 0-2	2.97	−0.03	-4.14	−0.14	4.83	−0.17
Element 0-3	3.08	0.08	-3.99	0.01	5.04	0.04
Element 1-1	2.93	−0.07	-4.04	−0.04	4.87	−0.13
Element 1-2	2.94	−0.06	-4.01	−0.01	5.15	0.15
Element 1-3	2.85	−0.16	-4.17	−0.17	5.14	0.14

Table 5.1: Measured angles after the adjustment process compared to their set-angles roll (3°), pitch (−4°) and yaw (5°) respectively. All units in degree.

	X_{ideal}	X_{meas}	Δ_X	Y_{ideal}	Y_{meas}	Δ_Y	Z_{ideal}	Z_{meas}	Δ_Z
Element 0-1	110.00	110.00	0.00	0.00	0.00	0.00	-453.00	-453.00	0.00
Element 0-2	328.63	328.60	−0.03	19.13	19.47	0.34	-437.65	-437.73	−0.07
Element 0-3	543.17	543.13	−0.03	56.27	56.27	0.00	-406.12	-405.73	0.38
Element 1-1	110.00	110.00	0.00	0.00	0.00	0.00	-453.00	-453.00	0.00
Element 1-2	328.63	328.66	0.03	19.13	18.64	−0.49	-437.65	-437.51	0.15
Element 1-3	543.17	543.15	−0.02	56.27	55.89	−0.38	-406.12	-405.77	0.35

Table 5.2: Comparison of the ideal TCPs calculated from set-angles to the measured TCPs calculated from measured angles. All units in mm.

0.49 mm). It should be noted, that the roll angle deviations do not have an impact on the accuracy of the ball joint TCPs, since it is the last rotation according to the Euler convention and describes the rotation about the X-axis. This results from the fact, that the transformation to calculate the following TCP is solely a translation along the X-axis of the measured TCP of the previous element. However, the roll angle deviations do have an impact on the accuracy of the gripping points below each element, which are important during pick and place operations. Therefore, the deviation of the roll angle has a negative effect when picking up fabric layers and placing them into the mold. Additionally, it should be noted, that the TCP of the innermost element is always fixed to the center element, and thus its position is always equal to the ideal TCP, as shown in table 5.2 for element 0-1 and element 1-1.

Further, the data shows an increasing error of the TCPs for the outer elements. This behavior is expected, since the angular deviations of the previous elements add up and displace the TCPs of the following elements. Occasionally, the angular deviations of following elements compensate each other (opposite sign), as can be observed for example from the Y-values of element 0-2 to element 0-3. As a consequence, the displacement for that axis decreases. At the same time, this shows the limitation of the current adjusting process, since the orientation of an element is not adjusted a second time, to correct a measured angular deviation of a joint.

5.2.5 Cooperative layup

In order to test the entirety of the system, the automated adjusting process was integrated into the fully automated pick and place process with two cooperating robots, for which the adjustments of the end-effectors were previously performed manually [5]. For that purpose, the set-angle determination from CAD, as described in section 4.2, was used. The end-effectors were adjusted separately to the calculated set-angles by the automated adjusting process, as described in section 4.1. Thus, the experiment serves as a test to verify the functional interaction of all hardware components and implemented software improvements. Additionally, the experiment was used to validate the set-angles determined from the surface geometry in CAD.

The experiment showed, that draping of the carbon fabric layers was possible during pick up motion, which requires a precise adjustment of the end-effector. Thus, the experiment proved, that the current accuracy of the adjusting process is sufficient for the draping process. Further, a large fabric layer was transported cooperatively by the robots to the mold and placed down. As seen in figure 5.6, the layup process of the carbon fabric was successful, thus both end-effectors are accurately adjusted to the double curved surface geometry of the mold. As a consequence, the set-angles determined in CAD are correct.
Additionally, the process was tested with a smaller edge piece of the preform, which required both end-effectors to be adjacent to one another and thus operate very close to each other. This requires a higher demand for accuracy and synchronization, as compared to handling large plies. During the experiment, it became evident, that draping during pick-up was possible, but the layup process has shown to be difficult, due to a high risk of collision. Synchronization of the robot's movement was an issue, but the root cause has not been determined yet.

However, the successful layup experiment for large plies proves the functional principle of the adjusting process. As a consequence, the set-angle determination is working, thus the process can be executed with sufficient accuracy for large carbon plies. Improvements to the hardware state may increase the accuracy even further, and enable the handling of small carbon plies as well.

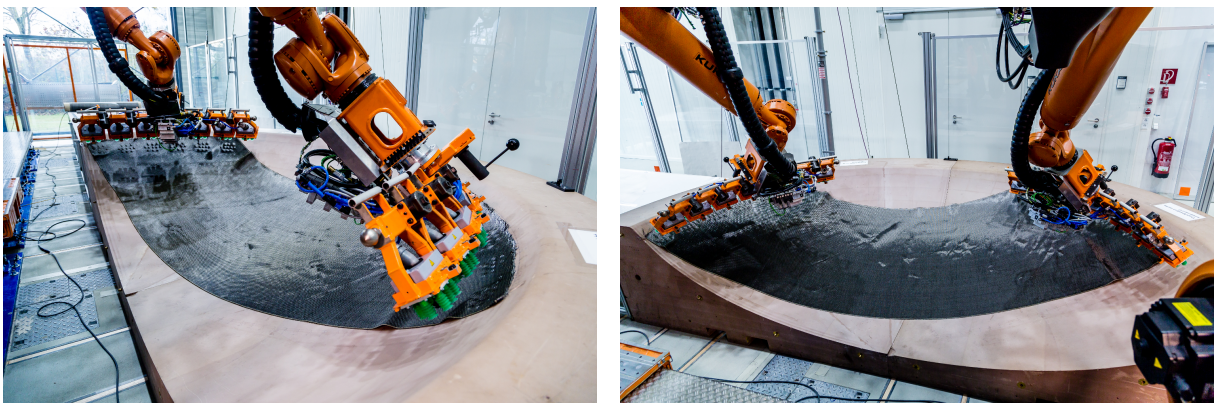

Figure 5.6: Successful cooperative layup of a large layer of carbon fabric into the mold.

5.3 Results and discussion

The first experiment showed a discrepancy of 0.248 mm in Y-direction between the measuring tubes of the innermost elements on each end-effector side. If not accounted for, this results in an angular measurement deviation of 0.13°. Hardware inaccuracies of the robotic end-effector would explain this observation. At the same time, this shows that the software calibration is necessary to reliably determine the reference point, in order to accurately calculate the roll angle deviation, although it can only be used to calibrate the innermost element on each end-effector side. On the other hand, this raises the question of whether more hardware inaccuracies are present, that can not be determined with the current measuring solution (e.g. for the outer elements).
During the adjusting process in the fourth experiment, it became evident, that the bottom surface of each element is not precisely parallel to the supporting surface of the adjusting station after the measuring process. However, the measurement inaccuracy of the measuring process has shown to be negligible (maximum standard deviation of 0.019°) for small angular deviations ($(< 0.2°)$), which are expected during normal operation. This yields the conclusion, that small angular deviations between the measuring tube and the bottom surface exist. As a consequence, an inaccurate alignment of the bottom surface to the base coordinate system can be observed. In conclusion, hardware inaccuracies must exist, which have a negative impact on the accuracy of the system throughout the process. Especially, any misalignment between the bottom surface and the supporting surface of the adjusting station creates unwanted movement (lateral shift) of each element when locking the clamping jaws. This causes stress on the mechanical components and leads to inaccurate adjustments. As a result, infrequent adjustment deviations of up to 0.17° occur, which result in an imprecise TCP calculation of up to 0.49 mm for the outer elements. This has a negative influence on the accuracy of the system, due to the fact, that rotations are not executed precisely about the center of the ball joint, which causes deviations in the adjusting and alignment motions of the robot. This effect is expected to be worse for the outer elements, which are at the end of the kinematic chain and influenced by the angular deviations of the previous elements. Remeasuring the element after the adjusting process helps to correct the calculation of the TCP position of the following element, but does not eliminate the root cause of this problem.
However, the final experiment showed, that the accuracy of the current system is sufficient to pick and place fabric layers, despite the imperfect hardware state, that negatively affects the process. In order to validate the absolute accuracy of the adjusting process, an external measurement solution should be used, such as a laser tracking system with a separate measuring probe [16].

Alternative measuring solution
If future experiments reveal, that the absolute accuracy of the measuring process is insufficient, a new measuring solution could be implemented, that relies on laser distance sensors instead of retro-reflective sensors. For that purpose, four measurement points on the side of each element could be obtained to calculate the angular deviation for the yaw and roll angle, and two additional measurement points on the top surface to determine the pitch angle. Correspondingly, the

top surface of each element has to be parallel to the bottom surface and the side surface has to be perpendicular to the bottom surface. As a result, rendering the measuring tube redundant, which presumably causes the inaccuracies throughout the process. The new measuring surfaces need to be planar, in order to ensure a precise measurement. This could be achieved accurately with a CNC machine, and applied to the current end-effector. The advantage of this solution is, that the measurement points can be obtained without a linear approach movement, solely by positioning the element accordingly, thus decreasing the process time of the measuring process. Further, the roll measurement does not rely on a fixed reference point, thus calibration is not required. Also, the angular deviation measurements should be independent of each other, since the accuracy of the roll angle measurement does not rely on the pitch and yaw angle measurement. Finally, the high accuracy of laser distance sensors should improve the accuracy of the measuring process.

Chapter 6

Conclusion

In this thesis, an automated measuring and adjusting process was developed and implemented that is capable of adapting the shape of the presented robotic end-effector to double curved surface geometries. The evaluation in a realistic production environment revealed, that the principle of the developed process is functionally adequate. Additionally, the cooperative layup experiment showed, that the set-angles can be accurately determined from CAD. Thus, the developed software serves as a link between the design and manufacturing of the component, that is necessary for an automated production process.
During the experiments, it turned out, that the accuracy of the system is currently limited by the state of the hardware. A software calibration method has proven to be successful in enhancing the performance of the measuring system, by determining the lateral offset of the measuring tubes. Despite that, further deviations in the hardware exist, that can not be compensated by the current measuring technique and cause inaccuracies in the final shape of the adjusted end-effector. However, deviations between the CAD model of the end-effector and the reality are expected and can be measured externally and integrated into the process.
Nonetheless, even in its current state, the precision of the adjusting process is sufficient to drape dry textiles during pick-up and create layups of large fabric layers with cooperating robots. As a consequence, the automated adjustment process can be integrated into the fully automated process for future layup experiments. Thus, the research conducted in this work, aims towards an automated manufacturing process that can be used to full-fill the increasing production rates of aircrafts, which require the production of large double curved CFRP-components, such as rear pressure bulkheads.

6.1 Outlook

In order to further improve the accuracy of the system, either the deviations of the hardware have to be determined with an external measurement solution and compensated on the software side, or further improvements have to be made to the hardware. Firstly the calibration method should be improved to enhance the performance of the system. For that purpose, the angular deviations and translatory offsets of the measuring tube to the bottom surface need to be determined for

each element. This could be achieved with an external measurement solution, such as a laser tracking system. These calibration values have to be included into the robot program, to ensure that the support surface of the adjusting station and the bottom surface of each element are parallel to each other after the measuring process. Additionally, the laser tracking system should be used to find the relative position between the element and the guiding pins of the clamping jaws, in order to determine the clamping position. This should further decrease the lateral shift in position of the elements, when locking the clamping jaws.
Additionally, the distance between each ball joint along the X-axis should be measured, to ensure an accurate TCP calculation for all elements, which potentially negatively affects the process.
Finally, base calibration should be executed automatically, since the manual measurement of the base poses an inaccuracy, which influences the whole process chain of the implemented process. The apparatus for automated base calibration is already provided and could be used to acquire a higher accuracy.
With these improvements, the precision of the adjusting process should be sufficient, so that the re-measurement of each element after the adjustment could be avoided and process time could be decreased.

Appendices

Appendix A

Documentation

A.1 Parameter of the robot program

The following section gives an overview of the parameters and variables of the robot program for future reference.

Variable name	Value	Description
D_TCP_TO_TCP_X	220	Distance from TCP (ball joint) to TCP (ball joint) along X-Axis (in mm).
D_FLANGE_TO_JOINT_Z	453	Distance from flange to ball joint along Z-axis (in mm) with multi-sided probe.
D_JOINT_TO_CENTER_X	110	Distance from ball joint to center of element along X-Axis (in mm).
D_JOINT_TO_TUBE_Z	112.5	Distance from ball joint to tube along Z-Axis (in mm).
D_JOINT_TO_GRIPPOINT_Z	257.499	Distance from ball joint to grip point TCP along Z.
D_JOINT_TO_BOTTOM_Z	258.300	Distance from ball joint to bottom of module along Z-Axis (in mm).
D_TUBE_LENGTH	160	Lengths of measuring tube (in mm).
D_TUBE_DIAMETER	25	Diameter of measuring tube (in mm).
D_MARGIN	100	Safety margin/buffer to avoid collision with adjusting station during approach movement (in mm).
D_SAFETY_HEIGHT_Z	1285.44	Safety height Z above base (in mm), where no collision with station is possible.

Continued on next page

Table A.1 – continued from previous page

Variable name	Value	Description
D_MEAS_VARIANCE_X	40	Half of the absolute distance about which measuring pre-positions are varied along X-Axis for measuring process (in mm).
D_SEARCH_LENGTH	125	Maximum length of linear search movement to prevent collision with adjusting station (in mm).
eps	0.5	Maximum allowed angular deviation after the measuring process (in degree).
V_SENSOR_X_ANGLE	10	Tilt angle offset of the vertical sensor about X-axis (in degree).
preClampPoseOffset_Z	50	Offset above clamping position of adjusting to slow down approach velocity (im mm).
measVel	0.02	TCP velocity during linear search movement during measuring process (in $\mathrm{m\,s^{-1}}$).
adjApprVel	0.25	Fast approach velocity to lower element to clamping pre-position (in $\mathrm{m\,s^{-1}}$).
adjApprVelSlow	0.01	Slow approach velocity to lower element onto final clamping position (in $\mathrm{m\,s^{-1}}$).
slowRotVel	3	Maximum rotation speed during adjusting process (in degree per second).
apprRotVel	20	Maximum rotation speed to perform 180° rotation to change end-effector side (in degree per second).

Table A.1: Parameters of the robot program in parameter.dat

Debug Option	Type	Description
debug_WithoutPressure	Bool	If true, allows to run the program without pressure, no adjustments are executed in this mode.
debug_manualWrenchCtrl	Bool	If true, loosening and tightening of the joint has to be performed manually. The program stops and displays a message that has to be confirmed, before the adjusting rotation movement is executed and after it finished, in order to tighten the joint.
debug_repeatMeasAfterAdj	Bool	If true, repeats the measuring process of the same element after adjusting process to correct TCP calculation of the following element.
debug_checkAdjPos	Bool	If true, program is halted before clamps close. Can be used to manually determine the clamping position.
debug_ShowInterruptPos	Bool	If true, halts the program at the sensor interrupt position.
debug_BusSystem	Bool	Should be set to true, if sensors are not connected via fast measuring lanes, but slower bus interface.
debug_straight	Bool	If true, assumes a straightend end-effector, overrides set-angles of previous end-effector state to 0.

Table A.2: Debug options of the robot program in debugOptions.dat

Variable name	Type	Description
endEffector[2,3]	ELEMENT_T	Stores the set-angles (roll, pitch, yaw) and the tool coordinate system (TCS) for each element in an array structure. Array size defined by: side (always 2), number of elements per side (changeable depending on hardware state). The TCS is calculated internally.
prevEndEffector[2,3]	ELEMENT_T	Stores a copy of the same data structure for the orientation of each element after the adjusting process.

Table A.3: Set-angle input in rpyJointParameter.dat

A.2 Electrical and mechanical controlling

Overview of the I/Os defined in WorkVisual for the KRC to control the adjusting station.

A.2.1 KRC inputs

Signal name	Index	Description
in_b6barOk	257	Pressure sensor - true if 6 bar are available.
in_clamp1Opened	259	True if clamp 1 is opened.
in_clamp1Closed	260	True if clamp 1 is closed.
in_clamp2Opened	261	True if clamp 2 is opened.
in_clamp2Closed	262	True if clamp 2 is closed.
in_wrenchArmDetached	263	True if tightening spindle arm is detached (ready to lower into adjusting station).
in_wrenchArmAttached	264	True if tightening spindle arm is attached (ready to start screw cycle).
in_CS351Ready	273	True if tightening spindle control system is ready.
in_CS351NoFault	274	True if tightening spindle control system is not in a faulty state.
in_CS351AckProgNo	275-276	Index of screw cycle program.
in_CS351InCy	277	True during screw cycle program.
in_CS351CyCmp	278	True after screw cycle is complete.
in_CS351ResOk	279	True if screw cycle was completed successfully.
in_CS351ResNok	280	True if screw cycle was not completed successfully. (error handling)

Table A.4: Input signals of the KRC defined in WorkVisual.

A.2.2 KRC outputs

Signal name	Index	Description
out_b6bar	340	Open/close safety valve.
out_closeClamps	341	Close clamping jaws.
out_openClamps	342	Open clamping jaws.
out_attachWrenchArm	343	Attach tightening spindle arm.
out_detachWrenchArm	344	Detach tightening spindle arm.
out_CS351Enable	345	Enables/switches on tightening spindle control system.
out_CS351ProgNo	346-347	Sets program number of screw cycle (2 bit).
out_CS351Tighten	348	Activates screw cycle to tighten the joint (clockwise rotation).
out_CS351Loosen	349	Activates screw cycle to loosen the joint (counter-clockwise rotation).
out_CS351ResetResult	350	Resets result (ResOk, ResNok) of previous screw cycle state.
out_CS351ResetFault	351	Resets the system error from a faulty state.
out_CS351NotOkAck	353	Acknowledges scre cycle Not Ok state.

Table A.5: Output signals of the KRC defined in WorkVisual.

A.2.3 Tightening spindle control diagram

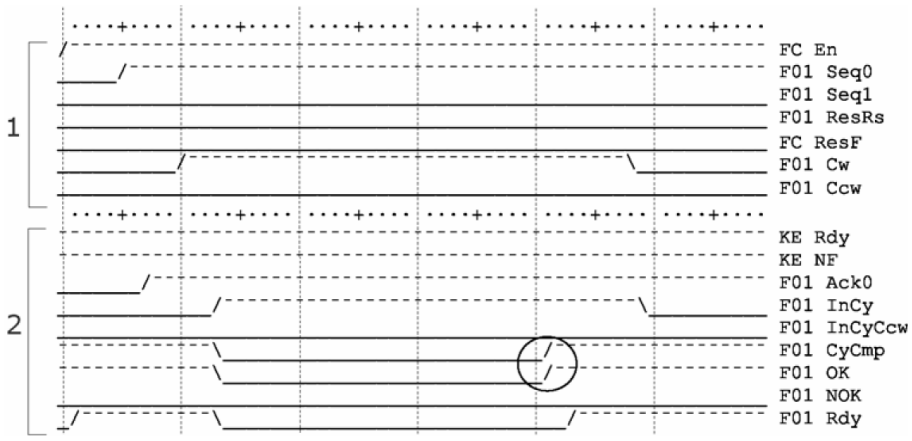

Figure A.1: Control diagram of the tightening spindle to perform a clockwise screw cycle rotation to tighten the joint [4].

A.3 Overview of additional hardware components

A.3.1 Tightening spindle

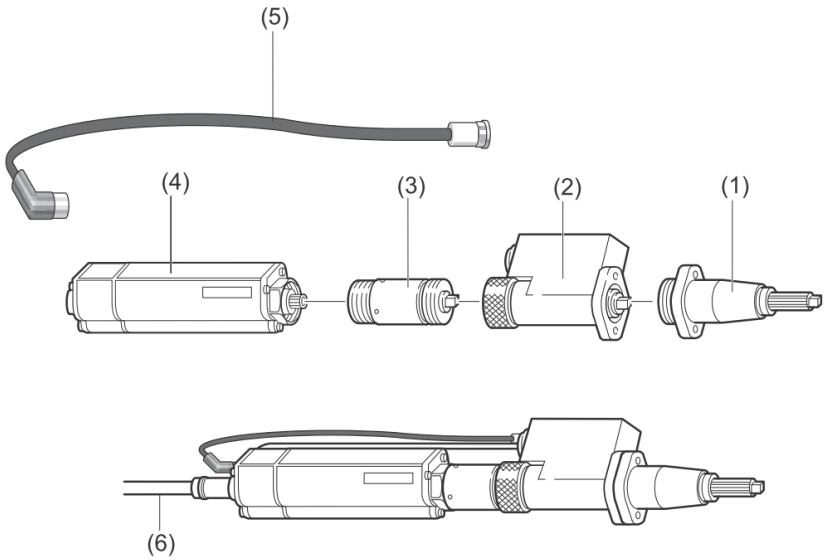

Figure A.2: Hardware components of the modular tightening spindle: Output drive (1), measurement transducer (2), planetary gearbox (3), EC drive unit servomotor (4), measurement transducer cable (5) and connecting cable to control system (6) [4].

A.3.2 Set-plate for manual adjustment

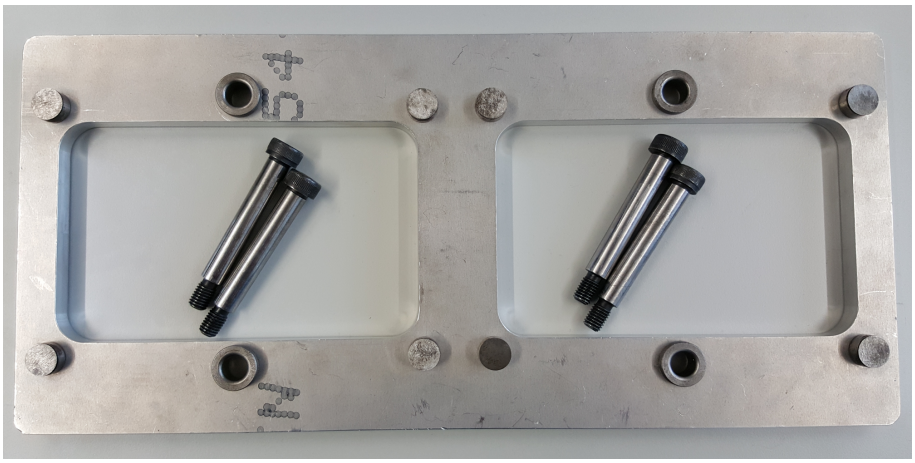

Figure A.3: Set-plate to align two consecutive elements of the end-effector parallel to each other by inserting the four shoulder bolts into the fixing collar bushings on the sides of each element and the set-plate.

List of Figures

List of Tables

List of Acronyms

CAD	Coumputer-aided design
CFRP	Carbon fiber reinforced plastic
CP	Continuous path
DoF	Degrees of freedom
I/O	Input and Output
IDE	Integrated development environment
KRC	KUKA Robot Control
KRL	KUKA Robot Language
PTP	Point-to-point
TCP	Tool Center Point
TCS	Tool Coordinate System

Bibliography

[1] Airbus. Orders and deliveries. http://www.airbus.com/content/dam/corporate-topics/publications/o&d/ODs_Airbus_Commercial_Aircraft_December_2017.xls, December 2017. last accessed: 18.01.2018.

[2] Airbus. Airbus to boost A320 production to 60 a month in mid-2019. http://company.airbus.com/news-media/press-releases/Airbus-Group/Financial_Communication/2015/10/20151030_airbus_production_rate_a320.html, 2018. last accessed: 18.01.2018.

[3] Beckhoff Automation. EtherCAT - Ethernet for Control Automation Technology. www.ethercat.org/en/technology.html, 2018. last accessed: 15.01.2018.

[4] Bosch. Rexroth Tightening Spindle - Installation Instructions. http://www.boschrexroth.com/various/utilities/mediadirectory/download/index.jsp?object_nr=36088700D0, 2018. last accessed: 21.01.2018.

[5] Lars Brandt and Mona Eckardt. Automated handling and positioning of large dry carbon fibre cut-pieces with cooperating robots in rear pressure bulkhead production. In *CEAS Aerospace Europe*, 2017.

[6] S. Briot and W. Khalil. *Dynamics of Parallel Robots: From Rigid Bodies to Flexible Elements*. Mechanisms and Machine Science. Springer International Publishing, 2015.

[7] Quingzheng Cheng. *Fiber-reinforced Composites.* Materials Science and Technologies. Nova Science Publishers, Inc, 2012.

[8] Marian Körber Christoph Frommerl. Comparison of fibre angles between hand draped carbon fibres and draping simulation. 8th International Symposium on NDT in Aerospace, November 2016.

[9] Dominik Deden. Entwicklung einer mobilen Plattform für die Justage eines rekonfigurierbaren Roboterendeffektors zur Handhabung textiler Halbzeuge (Developement of an automated adjustment station for a passive adjustable gripper used for handling of dry carbon fibre textiles). July 2015.

[10] J. Denavit and R. S. Hartenberg. A kinematic notation for lower-pair mechanisms based on matrices. *Trans. ASME E, Journal of Applied Mechanics*, 22:215–221, June 1955.

[11] Mona Eckardt, Andreas Buchheim, and Tobias Gerngross. Investigation of an automated dry fiber preforming process for an aircraft fuselage demonstrator using collaborating robots. *CEAS Aeronautical Journal*, 7(3):429–440, September 2016.

[12] KUKA. *Operating and Programming Instructions for System Integrators.*

[13] KUKA. *RoboTeam 2.0 manual.*

[14] KUKA. Work Visual. `www.kuka.com/de-de/produkte-leistungen/robotersysteme/software/systemsoftware/kuka_systemsoftware/kuka_work-visual`, 2018. last accessed: 08.01.2018.

[15] Lars Larsen and Georg Braun. Entwurf und Test eines Saugsystems für das automatisierte Handling von Kohlefasergelegen (Design and test of a suction system for automated handling of dry carbon fiber fabrics). confidential, 2011.

[16] Leica. Laser tracker systems. `http://www.hexagonmi.com/products/laser-tracker-systems`, 2018. last accessed: 21.01.2018.

[17] Stepan Lomov. *Non-Crimp Fabric Composites - Manufacturing, Properties and Applications.* Woodhead Publishing, 2011.

[18] A.C. Long. *Composites Forming Technologies.* Woodhead Publishing Series in Textiles. Elsevier Science, 2014.

[19] George Marsh. Airbus A350 XWB update. *Reinforced Plastics*, 54:20–24, 11 2010.

[20] Steffen Ropers. *Thermoplastic Prepregs*, pages 5–20. Springer, 2017.

[21] Danyal Sener. Handling von Faserhalbzeugen in der automatisierten CFK-Produktion (Handling of fibre textiles within the automated production of CFRP). confidential, 2011.

[22] Bruno Siciliano and Oussama Khatib. *Springer handbook of robotics.* Springer, 2016.

[23] SICK. WT27L-2F430 manual. `https://www.sick.com/media/pdf/4/64/964/dataSheet_WT27L-2F430_1016019_de.pdf`, 2018. last accessed: 07.01.2018.

[24] Dassault Systemes. Delmia. `www.3ds.com/products/delmia/`, 2018. last accessed: 16.12.2017.

Proclamation

Hereby I confirm that I wrote this thesis independently and that I have not made use of any other resources or means than those indicated.

Würzburg, January 2018

Robin Leblebici